2016-01-01

Macro- And Mesoscale Analysis Of Connections Between The Cingulate Region And The Lateral Hypothalamic Area: Tracer Co-Injection And Chemoarchitectural Studies In The Adult Male Rat

Kenichiro Negishi
University of Texas at El Paso, knegishi@miners.utep.edu

MACRO- AND MESOSCALE ANALYSIS OF CONNECTIONS BETWEEN THE CINGULATE REGION AND THE LATERAL HYPOTHALAMIC AREA: TRACER CO-INJECTION AND CHEMOARCHITECTURAL STUDIES IN THE ADULT MALE RAT

KENICHIRO NEGISHI

Master's Program in Biological Sciences

APPROVED:

_____
Arshad M. Khan, Ph.D., Chair

_____
Karine Fénelon, Ph.D.

_____
Edward Castañeda, Ph.D.

_____
Charles H. Ambler, Ph.D.
Dean of the Graduate School

MACRO- AND MESOSCALE ANALYSIS OF CONNECTIONS BETWEEN THE CINGULATE REGION AND THE LATERAL HYPOTHALAMIC AREA: TRACER CO-INJECTION AND CHEMOARCHITECTURAL STUDIES IN THE ADULT MALE RAT

by

Kenichiro Negishi, B.S

THESIS

Presented to the Faculty of the Graduate School of

The University of Texas at El Paso

in Partial Fulfillment

of the Requirements

for the Degree of

MASTER OF SCIENCE

Department of Biological Science

THE UNIVERSITY OF TEXAS AT EL PASO

December 2016

Acknowledgments

I would like to thank the UTEP department of Biological Sciences for giving me a cozy place to further my education. It has been three years since Dr. Arshad M. Khan took the gamble of recruiting me to his team. Under his mentorship, I never felt like I was simply trying to graduate or produce solid work. Instead, my challenge was to learn how to appreciate our craft like he does. Thanks to him, I got the chance to meet from some of the most hard-working and dedicated people I know. Among them, I must thank Berenise De Haro for her being a phenomenal person to look up to, as well to Briana E. Pinales for her anxiolytic qualities and Ellen M. Walker for setting good examples. I also had no idea how fun teaching could be until I saw Anais "supermom" Martinez and Chris D'Arcy conduct their classes.

Some special thanks must go to the care and insight with which my committee members, Dr. Karine Fénelon and Dr. Edward Castañeda, corralled my project. I am also grateful that they were kind enough to sit down with me and untangle my ideas.

I was fortunate on many occasions, despite alienating myself through long hours in the lab, to still find warm meals waiting at home or mirthful companionship with my favorite people. I am certain that I would have spent more time contemplating my time investments if not for those occasions. My deepest gratitude goes to the Negishi family, Robert M. Garza and Devin L. Villalobos, for showing me the support I did not imagine to have.

Abstract

Hypothalamic research since the middle of the 20th century shaped the view that the lateral hypothalamic area (LHA) has a central role in controlling appetitive drives. The LHA is anatomically positioned to receive converging axonal inputs which relay information about the body's metabolic state as well as descending projections from the cerebral hemispheres, which encode cognitive and emotional states that influence feeding. Cerebral inputs are capable of initiating feeding despite the presence of competing satiety signals. Recent work has shown that medial prefrontal cortical areas can drive feeding in sated animals, possibly by engaging hypothalamic hypocretin/orexin (H/O)-expressing neurons, which are known to send projections to the cortex. Neuroanatomical tract tracing was used, in rats, to test the hypothesis that there are bidirectional monosynaptic connections between the medial prefrontal cortex and the lateral hypothalamic area. To further examine hypothalamic-cortical interactions, prefrontal targets of H/O-containing axons were described with cell-type precision by using immunohistochemistry and neuronal reconstructions. Collectively, these experiments produced the highest spatial resolution maps of prefrontal chemoarchitecture and connections with the LHA. Additionally, they provide novel probe targets for future functional studies, which includes a previously unappreciated connection between the infralimbic cortical area and the terete part of the hypothalamic tuberal nucleus.

Table of Contents

List of Tables

List of Figures

Chapter I: Introduction

I.1. General background and aims of this project

Homeostatically driven feeding is largely influenced by internal cues. Circulating hormones secreted by the digestive system and adipose tissue, or the absence thereof, can elicit the sensations of hunger and satiety. Perhaps more immediate to survival, however, is the need to rapidly cease ingestion in response to immediate threats; alternatively, animals capable of overeating or selectively targeting calorie-rich foods in anticipation of food scarcity. These examples involve behaviors opposing homeostatic trajectories and can therefore be categorized as non-homeostatic behaviors. Moreover, these behaviors rely on interpretations of external cues relayed by the cerebral hemispheres cognitive system.

Of clinical interest, the ability to non-homeostatically initiate and arrest feeding is likely important in the formation of maladaptive conditions such as obesity and anorexia nervosa. A fundamental understanding of the underlying mechanisms can therefore lead to better treatments for these conditions. This study will primarily focus on two brain regions which are critical for the expression of cortically-driven feeding: The lateral hypothalamic area (LHA) and the infralimbic area (ILA), a visceral sensory-motor area. Before addressing the aims of this project, we will discuss these two regions and their roles in feeding.

I.1.1. The lateral hypothalamic area and feeding. Hypothalamic research into feeding behaviors are dominated by two themes which were exposed by behavioral work from the mid-20th century. First, electrical stimulation of the lateral hypothalamus was shown to increase feeding and self-stimulation in rats (Hoebel and Teitelbaum, 1962; Delgado and Anand, 1953). The magnitude of stimulation-induced lever-pressing was also shown to be regulated by the metabolic state of the animal (Hoebel and Teitelbaum, 1962). It was understood at the time that the hypothalamus contained numerous fiber systems (Gurdjian, 1927), and that electrically induced feeding non-selectively engaged vast network of spatially overlapping circuits. However, the methodologies need to reliably untangle these structural underpinnings have not been available until recently. Another set of experiments by Grossman (1960) demonstrated that depositions of different

crystalline chemicals from the same cannulae in the hypothalamus could elicit feeding or drinking based on whether the deposits released norepinephrine or acetylcholine crystals, respectively. Taken together, these studies illustrate some of the central themes of hypothalamic research which I begin to address here with structural work. Specifically, they revealed that feeding-related hypothalamic regions contain overlapping, chemically-coded networks which are functionally heterogeneous and sensitive to metabolic states. These themes will be further elaborated upon in the next sections in order to better contextualize the research presented here.

I.1.1.1. Chemical coding of appetitive processes. The first evidence of phenotype-specific sub-networks within the LHA was provided by Grossman in 1960. Deposition of norepinephrine or acetylcholine into the same part of the LHA produced feeding or drinking behaviors respectively. Since then, a multitude of neuropeptide and neurotransmitter systems have been identified and are similarly embedded within the LHA. These are broadly categorized as orexigenic (neuropeptide Y, Agouti-related peptide, galanin, and melanin-concentrating hormone) or anorexigenic (cholecystokinin, corticotropin-releasing factor, and bombesin), depending on whether they promote or inhibit feeding (for review, see Berthoud, 2011). Of these, the work shown here will only focus on the hypocretin/orexin (H/O) system, which is more relevant to subsequent discussions on cortically-driven feeding.

I.1.1.2. The hypocretin/orexin system: Feeding or arousal?. H/O was independently discovered by two groups (Sakurai et al., 1998; de Lecea et al., 1998) and was noted for its ability to stimulate food consumption and for its almost exclusive production within cell bodies of the dorsomedial hypothalamic nucleus and the LHA. Subsequent anatomical studies revealed widespread connections throughout structures associated with feeding and arousal. H/O-immunoreaction (ir) axons can be found in distributed feeding-related regions such as the arcuate, the ventromedial, and the paraventricular hypothalamic nuclei (Peyron et al., 1998). H/O-ir axons also heavily project to the locus coeruleus, the raphe nuclei, and the pontine reticular formation (Peyron et al., 1998), suggesting a role in arousal and wakefulness. Indeed, H/O axons make somatic appositions with norepinephrine-containing cells in the locus coeruleus (LC) and bath

applied H/O increases LC neuronal firing (Horvath, 1999). It is important to note that although the H/O system is implicated in two broad functions, feeding and alertness, these functions are not mutually exclusive. The sleeping animal, after all, does not feed very much.

I.1.1.3. Melanin-concentrating hormone. In addition to being another orexigenic peptide, melanin-concentrating hormone (MCH) is remarkably similar to H/O in terms of its behavioral effects and anatomical targets. MCH expression increases with fasting and intracerebroventricular (ICV) injections of MCH dose-dependently activate feeding in sated rats (Qu et al., 1996) in both light-dark phases (Rossi et al., 1997). Interestingly, chronic MCH results in tolerance and does not affect normal body weight, suggesting MCH is a controller of food intake but not a regulator of body weight (Rossi et al., 1997). Like H/O, MCH cell bodies are most abundant in the LHA but extend further than H/O-ir cells rostrally and caudally; MCH-ir cells can also be found in structures dorsal to the LHA to include the zona incerta and the posterior hypothalamic nucleus (Hahn, 2010; Swanson et al., 2005). MCH function has also been extended to neuroendocrine function (see discussion by Cvetkovic, 2003; Knollema, 1992). Behavioral studies have demonstrated that MCH can produce anxiolytic effects (Monzon and De Barioglio, 1999) and modify memory retention (Monzon et al., 1999).

I.1.2. Cortical organization and cytoarchitecture-based localization. Isocortex (neocortex) is the most superficial part of the cerebrum. It is recognized across mammals as a multi-laminar (usually six-layered) sheet with alternating cell-dense and sparse bands. Korbinian Brodmann noted subtle variations on this six-layer theme and used them as a basis for histological parcellations for localization and identification with the hopes of establishing cortical homologies across species (Brodmann, 1909). Although the pursuit of direct homologies is especially problematic when comparing the prefrontal areas of rats and humans (for example, the rat frontal cortex lacks a layer IV, which is prominent in humans), the same cytoarchitecture-based parcellation approach is nonetheless indispensable for identifying stable regional boundaries.

Despite the seemingly uniform appearance in their laminar organization, isocortical areas participate in a wide range of functions. These specializations, as we now know, are the result

of regional differences of incoming and outgoing neuronal connections. Connectomic analysis reveals that isocortical areas organize into structural modules, or discrete clusters of highly interconnected nodes (Bota, 2015). It is also the case that subcortical efferents and afferents of a given cortical region are shared, by degree, with neighboring areas. Long-distance, tangential (or horizontal) connections have been identified in supragranular and, to a lesser extent in infragranular layers (Schwarz and Bolz, 1991). Given the extent of connectedness and gradients of subcortical afferents, functional attributions should resist the strict adherence to boundaries. Cytoarchitecture-based parcellations are nevertheless indispensable as stable cross-reference.

I.1.2.1. Polymodal association cortex and visceral sensory-motor areas. Alternatively known as the "medial prefrontal cortex", the cingulate region (CNG) is defined by terminal fields of projections from the mediodorsal nucleus of the thalamus (MD) (Krettek and Price, 1989). Ordered dorsoventrally, these include the dorsal and ventral anterior cingulate (ACAd and ACAv), the prelimbic (PL), and the infralimbic area (ILA). Ventrolaterally, these also include the orbital area (ORB).

The CNG has well-established roles in working memory, executive functions, and polymodal sensory integration (see Euston, 2012 for review). Examination of their outputs using anterograde tracing revealed the dorsal parts, ACAd and dorsal PL, project more to regions related to locomotion and visually-guided orientation whereas ventral parts, ventral PL, ILA, and ORB, target nodes associated with autonomic and emotional (limbic system) processing (Sesack et al., 1989; Balfour, 2006). Accordingly, the ACAd is associated with foraging (Blanchard and Hayden, 2014) and the ILA augments the motivational drive and the hedonic impact of food (Castro, 2014; Mena, 2011).

I.1.3. Cerebral hemisphere control of feeding. Cerebral influence over motivational drives has been recognized since the electrical self-stimulation experiments done by Olds and Milner (1954). They noted that electrical stimulation of the septal area produced the most robust lever-press responses. Since then, the nucleus accumbens (ACB) (Stratford and Kelley, 1999) and, more recently, the ILA (Mena et al., 2011) and bed nuclei of the stria terminalis (Jennings, 2013) have

been shown to regulate feeding, presumably by direct interactions with the LHA.

A wide set of neuropeptide systems associated with feeding make promising targets for cerebral hemisphere control of food intake. For that reason it is perhaps customary to contextualize LHA-directed findings with these groups (e.g., H/O and MCH). Recent findings seem to favor an even broader, neurotransmitter-based approach. Jennings et al. (2013) reported that optogenetic stimulation of GABAergic BST projections induced feeding in sated mice. Furthermore, these GABA projections functioned by inhibiting glutamatergic cells in the LHA. Subsequent optogenetic stimulation of LHA glutamatergic cells accordingly suppressed feeding. Although H/O or MCH cells were not directly part of this pathway, LHA glutamatergic axons were abundant in loci known to heavily express H/O and MCH (Jennings et al., 2013). Another set of studies by O'Connor et al. (2015) demonstrated rapid attenuation of feeding after optical stimulation of ACB D1 receptor-expressing neurons. Swift deactivation of feeding resulted from ACB GABA projections terminating on a subset of LHA GABA-positive neurons lateral to the fornix. Similarly, these projections did not synapse onto MCH or H/O cells but instead functioned through what seemed to be a local disinhibitory circuit. It remains to be seen, however, if these neurons interact with the H/O and MCH systems nonetheless.

Cortically driven appetitive behaviors are also observed after associative learning with Pavlovian conditioning. Sated rats readily feed when food-paired tones are played (Petrovich et al., 2005). Under the same model, rats presented with the conditioned cues also showed increased activation of H/O neurons (Fos induction) in a region-specific way (Petrovich et al., 2012). Subsequent work revealed selective recruitment of ILA and PL neurons as well as LHA H/O neurons after 10 days of cue-food conditioning when compared to earlier training days (Cole et al., 2015). This finding is in line with the view that CNG and VSM play a role in the retrieval of remote memories (Euston et al., 2012).

I.1.8: Aims of this project. Having discussed two neuropeptide systems and cerebral control of feeding, a unifying model of the LHA microcircuits responsible for appetitive and consummatory behaviors seems untenable. Nonetheless, recent behavioral findings involving an ILA-LHA

circuit remain to be reconciled with detailed anatomical analysis. Rigorous examination of ILA-LHA projections is needed to determine their termination sites within the LHA and, further, to phenotypically characterize their post-synaptic targets. As discussed, LHA neurons can be equally relevant to feeding whether they contain neuropeptides or simply signal using GABA or glutamate. Confocal analysis of putative post-synaptic cells can sufficiently, but not definitively, identify ILA targets within the LHA. Furthermore, target cells must also be mapped to a reference atlas. Recent connectional and behavioral studies have made clear that, despite close proximity, neighboring LHA subregions are connectionally and functionally distinct (Hahn and Swanson, 2010; Hahn, 2015).

The effects of H/O and MCH on cortical dynamics are also unclear. It is possible that these LHA-derived peptides are capable of optimizing network sensitivity for the detection of food-related cues. Indeed, blockade of hypocretin receptor type 1, but not type 2, in the CNG was shown to reduce the power of low- and high-frequency gamma oscillations (He et al., 2015). This observation, together with the mounting evidence that GABAergic interneuron populations are richly diverse and highly coordinated in the formation and maintenance of dynamic oscillatory states (Tamas et al., 1998; Klausberger et al., 2008), highlights the importance of identifying H/O and MCH targets within cortical interneuron populations.

Given these outstanding issues in our understanding of CNG–hypothalamic information transfer related to motivated behaviors, the following specific aims were addressed in this project:

S. Aim 1. ***To characterize medial prefrontal neurons that receive neural inputs from the hypothalamus.***

S. Aim 2. ***Characterizing the inputs and outputs of the infralimbic area with an emphasis on connections with the lateral hypothalamic area.***

Below, I present the results of this work in the form of a manuscript being submitted for publication. Within it, I first present a more focused treatment of the subject, and then proceed to describe and present the results of my experiments towards both aims.

I.2: Introduction to the Study

Behavioral flexibility, or the initiation of adaptive changes in ongoing behavior, depends on a rich supply of goal-relevant information. The rodent cingulate region (CNG; Brodmann, 1909; alternatively, the "medial prefrontal cortex") is anatomically positioned to integrate multimodal contextual information and is thought to orchestrate top-down control of neuronal activity (Miller and Cohen, 2001; Euston et al., 2012). CNG organization has been divided across a dorsoventral functional and anatomical gradient (Heidbreder and Groenewegen, 2003) with the dorsal CNG associated with the control of actions and the ventral with emotional/autonomic control (Euston et al., 2012). In line with this model, recent work has shown that chemical activation of the ventral, but not dorsal, CNG was sufficient to drive feeding in sated rats (Mena et al., 2011); a similar effect was demonstrated with optogenetic stimulation of the ventral CNG in mice (Land et al., 2014). Elucidating the structural underpinnings of these effects may reveal critical nodes for the initiation of feeding and contribute to a broader understanding of cortical contributions to the control of motivated behaviors.

Feeding that is CNG-driven likely involves bidirectional connections with the lateral hypothalamic area (LHA), a brain region associated classically with appetitive behaviors (Morgane, 1961; Hoebel and Teitelbaum, 1962). In support of this view, feeding elicited by learned contextual cues requires an intact CNG (Petrovich et al., 2007) and was shown to recruit LHA-targeting CNG projections (Petrovich et al., 2005). Moreover, feeding triggered by intra-CNG infusions and conditioned cues (Petrovich et al., 2012; Mena et al., 2013) induced Fos expression among hypothalamic neurons expressing hypocretin/orexin (H/O). The subsets of activated H/O neurons were found primarily within the medial division of the "perifornical region" of the LHA, suggesting functional heterogeneity within the H/O neuronal population. Whether the recruitment of H/O neurons by CNG outputs occurs through monosynaptic interactions has not yet been determined. Using neuronal pathway tracing techniques, investigations have described the afferent (Hoover and Vertes, 2007; Thompson and Swanson, 2010) and efferent (Sesack et al., 1989; Takagishi and Chiba, 1991; Vertes, 2004; Gabbot et al., 2005; Balfour et al., 2006) connections of the CNG.

However, CNG connections, specifically with the LHA have received considerably less attention despite their abundance and apparent regional specificity. A proposed spatial framework that parcels the LHA into 16 provisional cytoarchitecturally-defined regions (Swanson, 2004), has been used to produce high spatial resolution maps of chemically defined hypothalamic neuronal populations (Swanson et al., 2005; Hahn, 2010). Projections from neurons from some of these LHA subdivisions have also been characterized with targeted injections of cholera toxin β-subunit (CTb) and *Phaseolus vulgaris*-leucoagglutinin (PHA-L) (Goto et al., 2005; Hahn and Swanson, 2010, 2012, 2015). A holistic account of LHA connectional architecture will also require a similar treatment of other connected structures.

In addition to the visual clarity they provide for mapped data, standardized brain atlas levels can serve as a platform to compare information from multiple datasets (Khan, 2013; Hahn and Swanson, 2015). This advantage can be exploited to contextualize CNG macro-connections with the diverse cell types found in the CNG as in other expanses of cerebral cortex (Klausberger and Somogyi, 2008; Lodato and Arlotta, 2015). Information outflow from the CNG is relayed by pyramidal cells whose activity is in large part shaped by local inhibitory interneurons (Merchant et al., 2012). Although the diversity of inhibitory neurons is well understood in terms of their neurochemical, morphological and biophysical properties, their differential contributions to behaviors has been less clear. Recent innovations towards in vivo recording (Fujisawa et al., 2008) and optogenetic techniques (Pinto and Dan, 2015) are beginning to uncover the contributions of interneurons to attentional and working memory processes (Kim et al., 2016). The emerging roles of interneuronal subclasses prompt further examination into the structural features of these cell types, specifically towards understanding their connectivity with respect to projections from other brain regions. It would be interesting to know whether LHA neurons directly engage certain subsets of interneurons to control cortical information flow.

Here we performed double label immunohistochemistry to map the distributions of putative GABAergic interneurons in the CNG. Additionally, we examined these interneurons for putative H/O axo-somatic interactions. This information, in conjunction with connectional data from tract

tracing experiments, is essential for a better understanding of the cognitive systems and their contributions toward motivated behaviors.

Table 1: Neuroanatomical Abbreviations Used in This Study

AAA	anterior amygdalar area
ACAd	anterior cingulate area, dorsal part
ACB	nucleus accumbens
AHA	anterior hypothalamic area
AHNa	anterior hypothalamic area, anterior part
AHNc	anterior hypothalamic area, central part
AHNd	anterior hypothalamic area, dorsal part
AHNp	anterior hypothalamic area, posterior part
AMd	anteromedial nucleus, thalamus, dorsal part
AMv	anteromedial nucleus, thalamus, ventral part
ARH	arcuate hypothalamic nucleus
AV	anteroventral nucleus, thalamus
BA	bed nucleus accessory olfactory tract
BSM	bed nucleus stria medullaris
BST	bed nuclei stria terminalis
BSTal	bed nuclei stria terminalis, anterior division, anteromedial area
BSTif	bed nuclei stria terminalis, posterior division, interfascicular nucleus
BSTpr	bed nuclei stria terminalis, posterior division, principal nucleus
BSTse	bed nuclei stria terminalis, posterior division, striatal extension
BSTsz	bed nuclei stria terminalis, posterior division, cell-sparse zone
BSTtr	bed nuclei stria terminalis, posterior division, transverse nucleus
BSTv	bed nuclei stria terminalis, anterior division, ventral nucleus
CEAc	central amygdalar nucleus, capsular part
CEAm	central amygdalar nucleus, medial part
CNG	cingulate region
COAa	cortical amygdalar area, anterior part
COApm	cortical amygdalar area, posterior part, medial zone
CP	caudoputamen
cpd	cerebral peduncle
DMHa	dorsomedial hypothalamic nucleus, anterior part
DMHp	dorsomedial hypothalamic nucleus, posterior part
DMHv	dorsomedial hypothalamic nucleus, ventral part
em	extramedullary lamina, thalamus
fa	corpus callosum, anterior forceps
fx	columns of the fornix
GPe	globus pallidus, external segment
GPi	globus pallidus, internal segment
I	internuclear area, hypothalamic periventricular region
IAD	interanterodorsal nucleus, thalamus
IAM	interanteromedial nucleus, thalamus
ILA	infralimbic area
int	internal capsule
LHA	lateral hypothalamic area
LHAad	lateral hypothalamic area, anterior region, dorsal zone
LHAai	lateral hypothalamic area, anterior region, intermediate zone
LHAav	lateral hypothalamic area, anterior region, ventral zone
LHAd	lateral hypothalamic area, dorsal region

LHAjd	lateral hypothalamic area, juxtadorsomedial region
LHAjp	lateral hypothalamic area, juxtaparaventricular region
LHAjvd	lateral hypothalamic area, juxtaventromedial region, dorsal zone
LHAjvv	lateral hypothalamic area, juxtaventromedial region, ventral zone
LHAm	lateral hypothalamic area, magnocellular nucleus
LHAp	lateral hypothalamic area, posterior region
LHApc	lateral hypothalamic area, parvicellular region
LHAs	lateral hypothalamic area, suprafornical region
LHAsfa	lateral hypothalamic area, subfornical region, anterior zone
LHAsfp	lateral hypothalamic area, subfornical region, posterior zone
LHAsfpm	lateral hypothalamic area, subfornical region, premammillary zone
LHAvl	lateral hypothalamic area, ventral region, lateral zone
LHAvm	lateral hypothalamic area, ventral region, medial zone
MA	magnocellular nucleus
mct	medial corticohypothalamic tract
ME	median eminence
MEex	median eminence, external lamina
MEin	median eminence, internal lamina
MEAad	medial amygdalar nucleus, anterodorsal part
MEAav	medial amygdalar nucleus, anteroventral part
MEApv	medial amygdalar nucleus, posteroventral part
MPN	medial preoptic nucleus
MPNl	medial preoptic nucleus, lateral part
MPNm	medial preoptic nucleus, medial part
MPO	medial preoptic area
mtt	mammillothalamic tract
NC	nucleus circularis
NDB	diagonal band nucleus
NLOT	nucleus of the lateral olfactory tract
opt	optic tract
ORBv	orbital area, ventral part
PA	posterior amygdalar nucleus
PL	prelimbic area
PH	posterior hypothalamic nucleus
PR	perireuniens nucleus
PT	paratenial nucleus
PV	periventricular hypothalamic nucleus
PVa	periventricular hypothalamic nucleus, anterior part
PVi	periventricular hypothalamic nucleus, intermediate part
PVpo	preoptic periventricular nucleus
PVH	paraventricular hypothalamic nucleus
PVHap	paraventricular hypothalamic nucleus, anterior parvicellular part
PVHdp	paraventricular hypothalamic nucleus, dorsal parvicellular part
PVHf	paraventricular hypothalamic nucleus, forniceal part
PVHlp	paraventricular hypothalamic nucleus, lateral parvicellular part
PVHmpd	paraventricular hypothalamic nucleus, medial parvicellular part, dorsal zone
PVHmpv	paraventricular hypothalamic nucleus, medial parvicellular part, ventral zone
PVHpml	paraventricular hypothalamic nucleus, posterior magnocellular part, lateral zone
PVHpmm	paraventricular hypothalamic nucleus, posterior magnocellular part, medial zone
PVHpv	paraventricular hypothalamic nucleus, periventricular part

PVT	paraventricular nucleus, thalamus
RCH	retrochiasmatic area
RE	nucleus reuniens
REa	nucleus reuniens, rostral division, anterior part
REcd	nucleus reuniens, caudal division, dorsal part
REcm	nucleus reuniens, caudal division, median part
REcp	nucleus reuniens, caudal division, posterior part
REd	nucleus reuniens, rostral division, dorsal part
REl	nucleus reuniens, rostral division, lateral part
REm	nucleus reuniens, rostral division, median part
REv	nucleus reuniens, rostral division, ventral part
RH	rhomboid nucleus
RT	reticular nucleus, thalamus
ri	rhinal incisure
SBPV	subparaventricular zone
SCH	suprachiasmatic nucleus
SEZ/RC	subependymal zone/rhinocele
SI	substantia innominate or innominate substance
sm	stria medularis
SMT	submedial nucleus, thalamus
SO	supraoptic nucleus
SOr	supraoptic nucleus, retrochiasmatic part
st	stria terminalis
STN	subthalamic nucleus
sup	supraoptic commissures
TTd	tenia tecta, dorsal part
TU	tuberal nucleus
TUi	tuberal nucleus, intermediate part
TUl	tuberal nucleus, lateral part
TUsv	tuberal nucleus, subventromedial part
TUte	tuberal nucleus, terete part
V3h	third ventricle, hypothalamic part
V3t	third ventricle, thalamic part
VAL	ventral anterior-lateral complex thalamus
vlt	ventrolateral hypothalamic tract
VM	ventral medial nucleus, thalamus
VMHa	ventromedial hypothalamic nucleus, anterior part
VMHc	ventromedial hypothalamic nucleus, central part
VMHdm	ventromedial hypothalamic nucleus, dorsomedial part
VMHvl	ventromedial hypothalamic nucleus, ventrolateral part
ZI	zona incerta
ZIda	zona incerta, dopaminergic group

Chapter II: Materials & Methods

II.1: Animals

Experiments were performed on adult male Sprague-Dawley rats (Harlan Labs, Indianapolis, IN) weighing 300–350 g. Animals were fed ad libitum and housed in a temperature-controlled vivarium under a 12-hour day/night cycle. All methods followed protocols approved by the University of Texas at El Paso Institutional Animal Care and Use Committee.

II.2: Intracranial tracer injection

Rats were anesthetized with a mixture containing 50% ketamine, 5% xylazine, 10% acepromazine and 35% sterile saline at a dosage of 1 µL/g. Once anesthetized, animals were positioned in a Kopf stereotaxic frame and maintained under 1.5% isoflurane delivered with pure oxygen for the duration of the surgery. The frontal bone and bregma fiducials were carefully exposed for craniotomy. Glass micropipettes with inner tip diameters ranging from 12 to 20 µm were selected and filled with a cocktail of PHA-L (Vector Laboratories, catalog #L-1110) and CTb (List Biological Laboratories, catalog #104) dissolved in dibasic sodium phosphate solution. Stereotaxic coordinates targeting the ILA (AP +11.20 mm, ML –0.50 mm and DV –4.40 mm) and ACAd (AP +11.20 mm, ML –0.50 and DV –2.40 mm) were obtained using the Paxinos and Watson rat brain atlas (2014). Tracer was ejected iontophoretically at a current of 5 µA through 7 sec on/off cycles for a 10–15 min. Micropipettes were retracted slowly after a resting period of 10 min. Post-surgical animals received intramuscular injections of Flunazine (i.m., Bimeda-MTC Animal Health, Inc., catalog #200–387, lot #2K017) as an analgesic and GentaVed (i.m.; Vedco, Inc., catalog #50989-040-12, lot#110561) for its antimicrobial and anti-inflammatory properties. Another injection of Flunazine was given 8 h after surgery. Daily status evaluations were maintained for a survival period of 10–14 d to allow for tracer transport.

II.3: Transcardial perfusion and tissue preparation

Animals were sedated with isoflurane for two min and perfused transcardially with 150 mL of phosphate-buffered saline (pH 7.4 at room temperature), followed by fixation with 350 mL of ice-cold 4% paraformaldehyde (PFA) in 0.1 M sodium borate buffer (pH 9.5 at 4°C). Brains

and spinal cords were carefully dissected and post-fixed overnight in an aliquoted PFA solution containing 12% sucrose (w/v) at 4°C. Fixed brains were then blocked (a coronal cut at the level of the caudal end of the mammillary body) and frozen rapidly in hexanes cooled over dry ice. Blocks were cut into coronal sections of 30-µm thickness as six 1-in-6 series using a Reichert sliding microtome (Reichert Austria Nr. 15 156) equipped with a modified freezing stage (Brain Research Laboratories, Newton, MA; Cat #3488-RJ). Sections were collected into 24-well plates containing cryoprotectant (50% phosphate buffer, 20% glycerol, and 30% ethylene glycol) and stored at –20°C until further processing.

II.4: Tissue processing and immunohistochemistry

II.4.1: Immunohistochemistry.

Sections were removed from cryoprotectant and placed in an isotonic 0.05 M Tris-buffered saline (TBS; pH 7.4 at room temperature) for five washes, each for five min (5 x 5). For sections processed for staining with 3, 3'-diaminobenzidine (DAB), endogenous peroxidase activity was then suppressed with a TBS solution containing 0.014% phenylhydrazine for 20 min and then rinsed in TBS (5 x 5). All sections were then incubated for 1.5 h in a blocking solution consisting of 2% (v/v) normal donkey serum (EMD Millpore; Catalog #S30-100ML, Lot #2510142) and 0.1% Triton X-100 (Sigma-Aldrich; Catalog #T8532-500ML, Lot #MKBH4307V) in TBS. Next, sections were treated with a solution containing primary antibodies diluted in blocking solution according to parameters detailed in **Table 2**. Sections were then washed (5 x 5) in TBS and incubated in a cocktail containing secondary antibodies (**Table 2**). When required, sections were counterstained with fluorophore conjugates diluted in blocking solution (**Table 2**). After final washes in TBS (5 x 5), sections were mounted onto Superfrost slides, air-dried, coverslipped with sodium bicarbonate-buffered glycerol (pH 8.6 at room temperature), and sealed using clear nail polish.

II.4.2: Tracer detection

Injection sites for PHA-L and CTb were immunodetected in single-labeled sections. One series was washed in TBS (5 x 5) and transferred into a TBS solution containing 0.014%

phenylhydrazine for 20 min to suppress endogenous peroxidase activity. After another wash in TBS (5 x 5), sections were pretreated for 1.5 h in a blocking solution containing 2% normal donkey serum and 0.1% Triton X-100 in TBS. Next, sections were incubated in blocking solution with diluted antibodies raised against either PHA-L or CTb (**Table** 2) for approximately 3 d (60 h at 4°C). Sections were washed in TBS (5 x 5) and treated with HRP-conjugated secondary antibodies diluted in blocking solution (**Table 2**) for 5 h at room temperature. After TBS washes (5x5) sections were developed in 0.05% DAB (Sigma-Aldrich) mixed with 0.0001% H2O2 in 0.05 M TBS for 20 min. Sections were washed in TBS (5x5), mounted onto gelatin-coated slides and left to dry overnight at room temperature. Tissue sections were dehydrated with ascending concentrations of ethanol (50–100%), defatted in xylene, then coverslipped with DPX mounting medium (Catalog # 06522; Sigma-Aldrich).

Table 2. List of antibodies and reagents

Reagent	Antigen/Conjugate	Host	Type	Source	Titer	Incubation
Primary	PHA-L	Rb	polyclonal IgG	Vector Labs	1:4,000	60 h, 4˚C
	CTb	Gt	polyclonal IgG	List Biological	1:10,000	60 h, 4˚C
	hypocretin / orexin A (C-19)	Gt	polyclonal IgG	Santa Cruz	1:4,000	60 h, 4˚C
	parvalbumin	Ms	polyclonal IgG	Abcam	1:5,000	60 h, 4˚C
	somatostatin (H-106)	Rb	polyclonal IgG	Santa Cruz	1:1,000	60 h, 4˚C
Secondary	anti-rabbit IgG	Dk	Cy5-conjugated	Jackson	1:500	5 h, 22˚C
	anti-mouse IgG	Dk	biotinylated	Jackson	1:500	5 h, 22˚C
	anti-rabbit IgG	Dk	biotinylated	Jackson	1:500	5 h, 22˚C
	anti-goat IgG	Dk	biotinylated	Jackson	1:500	5 h, 22˚C
Conjugate	avidin	-	HRP-conjugated (ABC kit)	Vector Labs	1:500	1 h, 22˚C
	avidin	-	Alexa 488-conjugated	Invitrogen	1:500	1 h, 22˚C
Chromagen	DAB mixture	-	see footnote 1	Sigma-Aldrich	-	variable

1: Mixture contained 0.05% 3,3'-diaminobenzidine (DAB) solution containing 0.0001% H_2O_2 and 0.1% ammonium nickel (II) sulfate was added for heavy metal intensification.

II.4.3. Nissl staining

Sections were rinsed twice in isotonic TBS (pH 7.4 at room temperature) to remove cryoprotectant. Freely floating sections were mounted onto gelatin-coated glass slides and dried overnight (24 h) at 60°C. Sections were dehydrated through ascending concentrations of ethanol (50–100%; 3 min each), defatted in xylenes for 25 min, stained with a 0.5% thionin solution (thionin acetate, Catalog #T7029; Sigma-Aldrich Corporation, St. Louis, MO) and differentiated in 0.4% anhydrous glacial acetic acid. Stained slides were coverslipped with DPX mounting medium and left to dry overnight.

II.5. Photography and post-acquisition image processing

Immunostained CNG sections were visualized with epifluorescence illumination using a Zeiss M2 AxioImager microscope equipped with an X-Y-Z motorized stage (Carl Zeiss Corporation, Thornwood, NY). An EXi Blue camera (QImaging, Inc., Surrey, British Columbia, Canada) operated by Volocity Software (Version 6.1.1; Perkin-Elmer, Inc., Waltham, MA; installed on an Apple Mac Pro computer) was used to generate wide field mosaic images from multiple channels. The same equipment was used to generate bright field stitched images of adjacent Nissl-stained CNG sections. Images were adjusted for brightness and contrast using Volocity Software and exported to Adobe Illustrator (AI; Version CC 18.0.0; Adobe Systems, Inc., San Jose, CA) as lossless TIFF-formatted files.

II.6. Parcellations, image overlays and mapping of CNG chemoarchitecture

Adobe Illustrator (AI; version CC 18.0.0; Adobe Systems, Inc., San Jose, CA) was used to draw cortical parcellations as separate layers to imported Nissl layers. Laminar and regional boundaries were determined using the cytoarchitectonic criteria and nomenclature outlined in the Swanson rat brain atlas (2004). Photomicrographs of immunostained sections were then overlaid upon the Nissl image, primarily by aligning blood vessels that traversed the sections. Atlas level assignments were created as a separate layer. Immunostained cell bodies and fibers were represented on open-access AI files of atlas maps from Swanson (2004) in a manner that accurately represented spatial distribution, density, orientation and branching.

II.7. Mapping of immunohistochemically detected tracer

DAB- and Nissl-stained sections were visualized using an Olympus BX53 microscope equipped with a drawing tube. Nissl-defined boundaries within regions containing tracer were designated using the terminology and mapping approach described by Swanson (2004). Injection sites for both tracers, along with the locations of PHA-L-labeled axons and CTb-labeled neurons were drawn using the camera lucida method by consulting the adjacent Nissl-stained tissue sections. Plane of section and atlas level assignments were determined using Swanson (2004) as a reference. Tracer representations were transposed to open-access AI files of atlas plates from Swanson (2004; http://larrywswanson.com).

Chapter III: Results

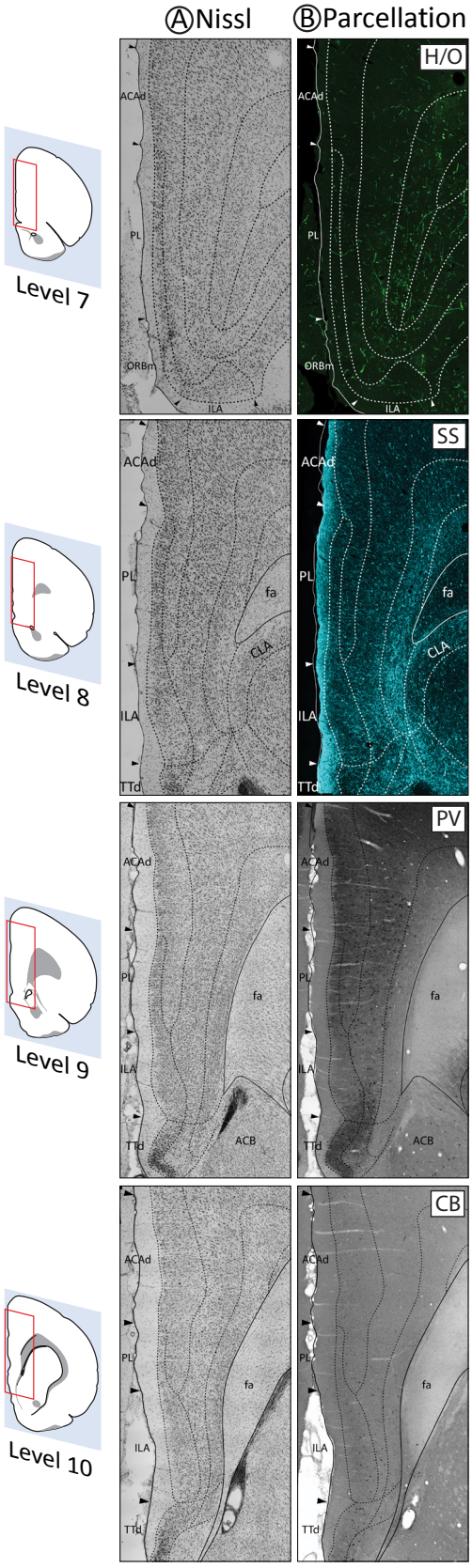

III.1. Aim 1: Mapping of CNG chemoarchitecture

Qualitative analysis of CNG chemoarchitecture was performed on atlas plates which included the rostrocaudal extent of the ILA (atlas levels 7–10). Spatial coordinates for data plotted to the atlas were derived using the cytoarchitectural criteria used by Swanson (2004) (**Figure 1A**), which draw from the studies by Krettek and Price (1977) and Vogt and Peters (1981). Briefly, the ILA is distinguishable from the dorsally adjacent PL by its unclear layer 1/2 boundary, cell groups in the deeper PL are also more densely packed. Dorsal to the PL, cells in the ACAd are less dense in layers 2, 5 and 6; this area is further elaborated by a pronounced columnar cell orientation. Boundaries established on the basis of the adjacent Nissl-stained section were overlaid on immunostained sections by using the camera lucida method or as separate layers of an Adobe Illustrator file (**Fig. 1B**). This basic approach was applied to determine the approximate locations for all mapped cell bodies reported in the present study.

< Fig. 1. Representative photomicrographs showing the basic mapping approach used to plot immunohistochemical data to atlas plates. (left) Illustrations showing regional approximations (red boxes) for adjacent photomicrographs. (A) Nissl-stained sections showing parcellations of the CNG using the criteria of Swanson (2004). (B) Adjacent CNG sections stained using immunofluorescent and immunoperoxidase reactions.

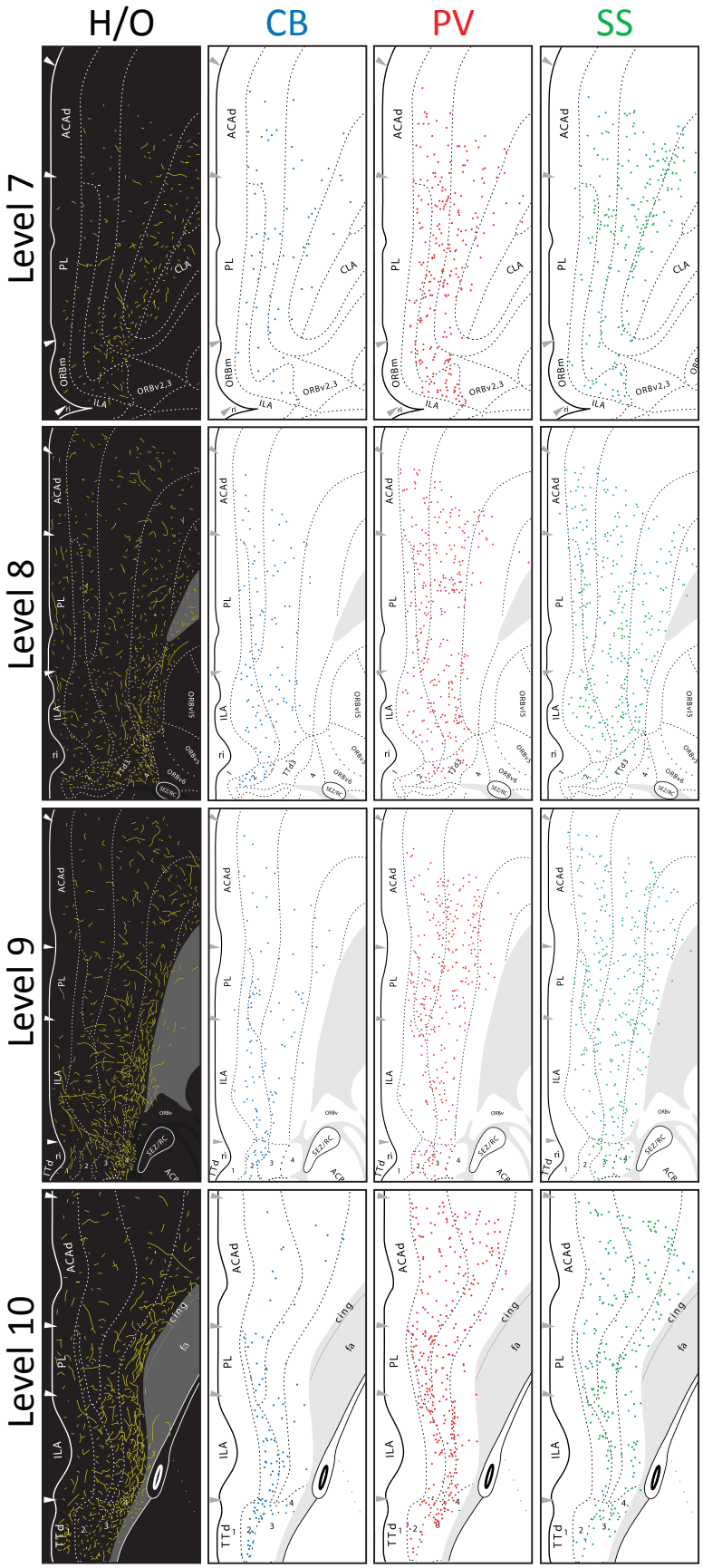

Close examination of presumptive GABAergic interneurons in the CNG revealed some distinct features. Notably, a density gradient was recognizable across the dorsoventral axis for each of the markers examined (**Fig. 2**).

SS- and PV-immunoreactive (-ir) cells displayed a reduced density in ventral parts of the CNG, particularly in the more caudal ILA. In contrast, CB-ir cells and H/O-ir axons were denser in the caudoventral CNG. These patterns were not observed in more rostral CNG areas we sampled, including

< Fig. 2. Representative maps of CNG chemoarchitecture. Locations of immunohistochemically labeled peptides were plotted using the approach described in Fig. 1. Maps were generated using sections stained for hypocretin/orexin (H/O; yellow) axons, and cell bodies labeled for calbindin (CB; blue), parvalbumin (PV; red) and somatostatin (SS; green) spanning levels 7–10 of the CNG. Atlas templates were taken from Swanson (2004; www.larrywswanson.com).

levels 7 and 8 (**Fig. 2**). Laminar patterns among immunodetected groups were also noted. H/O-ir axons were the only group regularly detected in layer 1. Labeled interneurons, along with H/O-ir axons, were observed to varying degrees in layers 2–6. Layer 6 was uniformly lacking PV-ir and CB-ir cells whereas the density of SS-ir cells was comparable in layer 6 as in layer 5. PV-ir cell density was selectively reduced in layer 2/3 of the caudal ILA whereas CB- cells were denser in the same region.

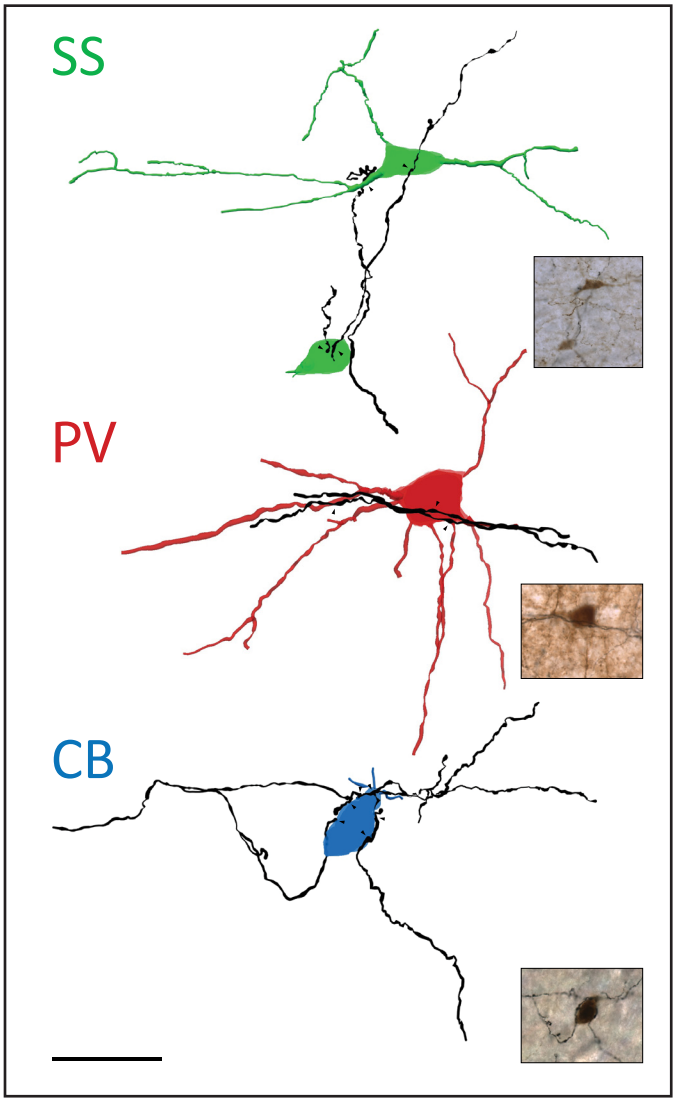

Fig. 3. Reconstructions of CNG neurons showing putative appositions (black arrowheads). Neurons are colored according to the scheme established in Fig. 2. H/O immunoreactive axons are drawn in black. The precise locations of neurons represented here are indicated by color-coded arrowheads in Fig. 4. Insets contain photomicrographs of reconstructed cells and processes. All reconstructions are drawn to scale (scale bar: 25 *μm*).

Interactions among H/O-ir and the interneuron groups were also examined within the same spatial framework. Dual-label immunohistochemical reactions demonstrated putative axo-somatic interactions between H/O-ir axons and with each of the interneuron groups. Demonstrative reconstructions for putative interactions are shown in **Fig. 3**. Most of the observed putative interactions consisted of one to three H/O-ir boutons except for a few which contained up to seven apposed boutons.

At a qualitative level, the spatial distributions of these groups correlated strongly with the distribution of H/O-ir axons (**Fig. 4**). Most putative appositions were detected in the ventral CNG as compared to the sparse interactions in the ACAd. Importantly, the lack of detectable

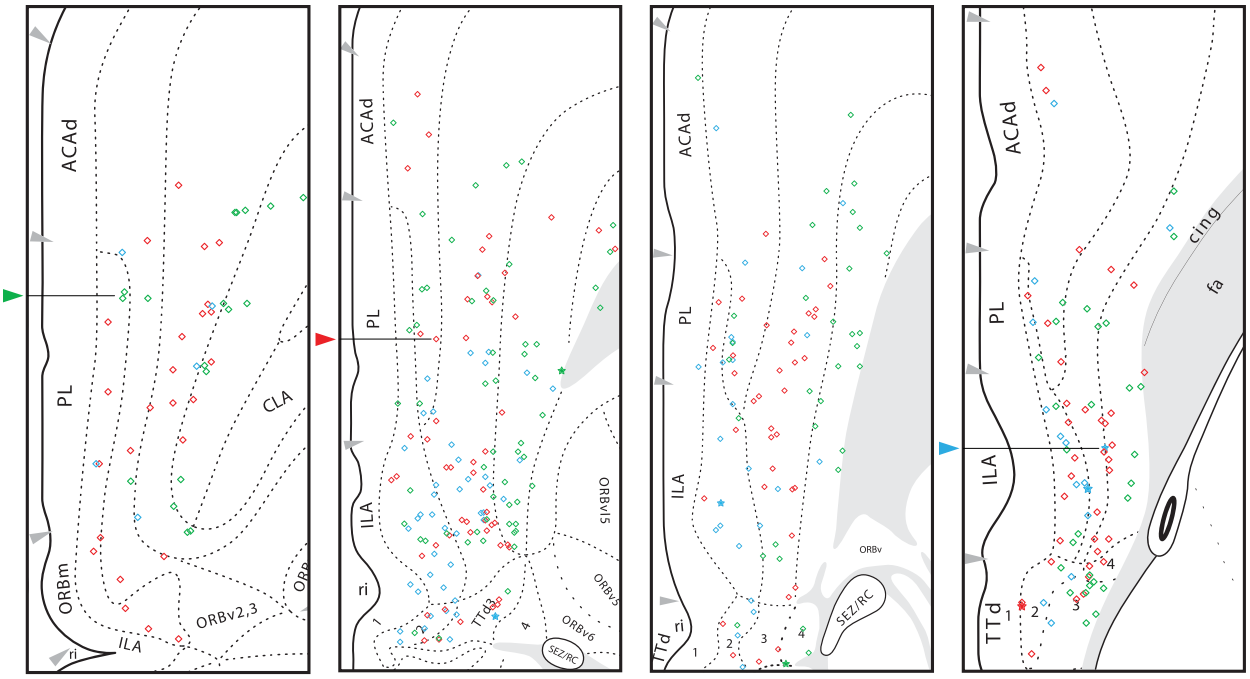

Fig. 4. Maps showing locations of putative appositions among H/O-labeled axons and chemically identified CNG cell types. Putative axosomatic interactions were detected using x63 magnification objectives and plotted as diamonds using the same color scheme as in Fig. 2. Green, red, and blue arrowheads mark the locations of neurons reconstructed in Fig. 3, and are color-coded to correspond to the color assignments for the various interneuron classes shown in Fig. 3.

---

interactions in the ACAd was not due to a general lack of immunodetected cells or H/O-ir axons.

III.2. Aim 2a: Neuroanatomical connections of the CNG

Previous tract tracing studies identified the ventral CNG structures as the primary sources of cerebral cortical projections to the LHA (Sesack et al., 1989; Vertes, 2004). To characterize these connections further, we targeted injections of anterograde and retrograde tracers into circumscribed CNG areas. Injection cases #15-072 and #15-113 are of interest to our analysis as they are contained within a midrostrocaudal to caudal part of the ILA. This region has recently been shown to control feeding (*see* **Discussion**) and is innervated robustly by H/O-ir axons (**Fig. 3**).

Immunodetected injection deposits sites for the tracers were located using the same approach as shown earlier for the CNG chemoarchitecture (*see* **Fig. 1**). Here, co-injected PHA-L and CTb are treated as separate cases because they differ in their diffusion profiles and uptake mechanisms (Gerfen and Sawchenko, 1984; Luppi et al., 1990) (**Fig. 5**). We found that co-injected tracers

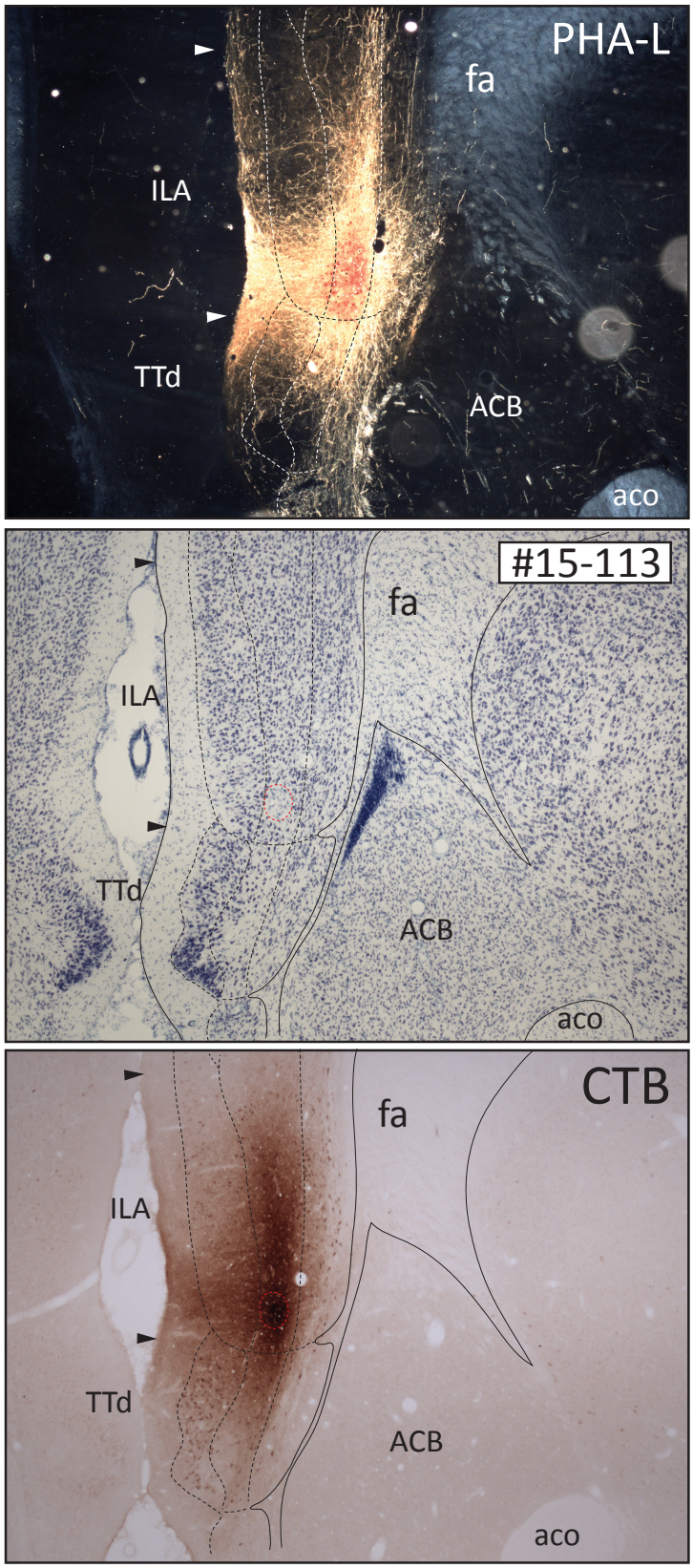

Fig. 5. Representative brightfield and darkfield photomicrographs showing the locations of immunodetected tracers in the CNG.

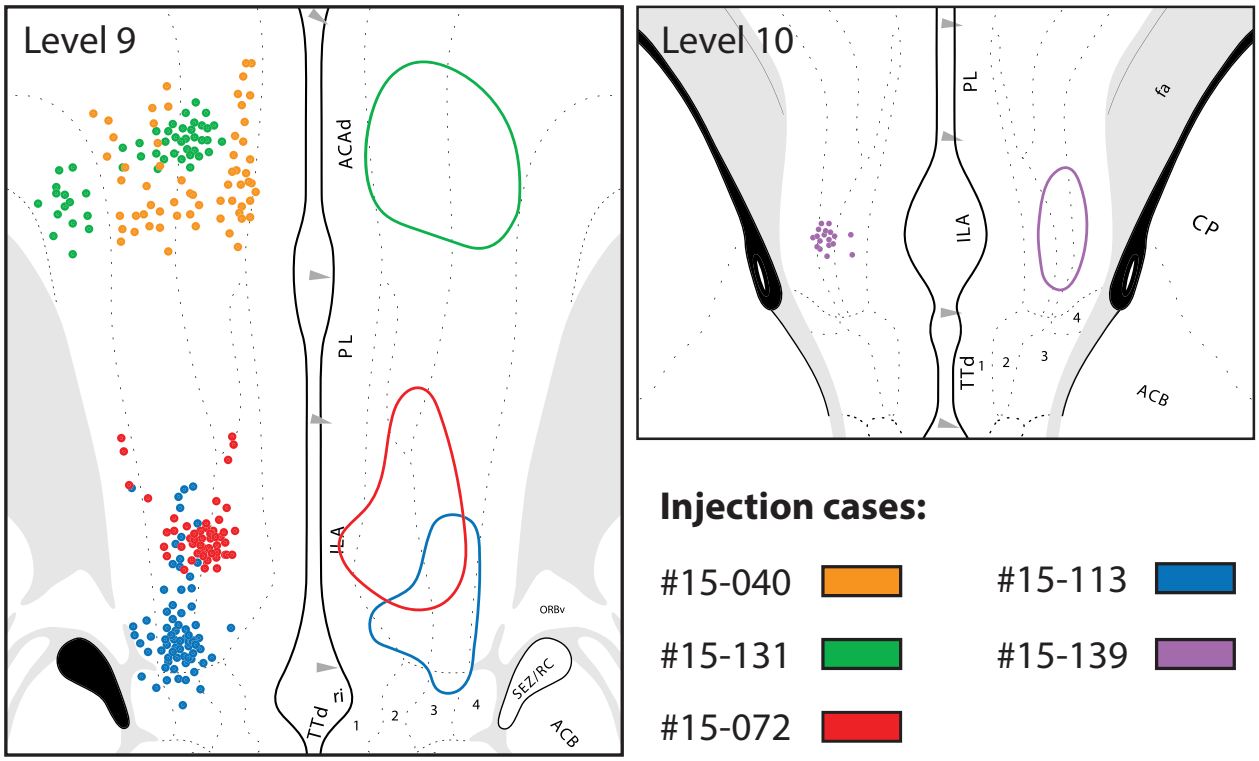

Fig. 6. Maps showing the locations of the injection sites for which anterograde and retrograde labeling was analyzed in this study. Two atlas levels (9 & 10) from Swanson (2004) are shown above. The full extent of the injection deposit is marked by colored outlines for CTb in the right hemisphere of each map, with corresponding cell bodies that were observed to take up the PHA-L tracer shown in the left hemisphere. Although these tracers are represented for the sake of clarity on separate hemispheres, they were injected together in the animal's right hemisphere. Colors denote specific patterns of injection deposits for separate animals, organized by case # in the legend.

---

largely overlapped in their distributions but marginal differences were also apparent.

From a total of 39 co-injection experiments, five were selected to investigate CNG connectional distributions within the LHA (**Fig. 6**). These include two injections centered in the ACAd and three injections centered in the ILA. It was clear from these experiments that CNG-LHA connections arose largely from the ILA and sparsely from the ACAd. Given this trend, a complete account of anterograde and retrograde tracer distributions in the LHA will be described for two injections centered in the ILA at level 9. Injection #15-072 is localized mostly to the dorsal part of the ILA but small amounts of tracer were also detected in the PL; case #15-113 was also in the ILA of level 9 albeit slightly more caudally and ventrally (**Fig. 6**).

III.2.1. Aim 2a: Projections from the ILA to the LHA (PHA-L anterograde tracing). At the level of the rostral LHA, descending axons distribute through two main white matter pathways. Labeled axons in both cases (#15-072 and #15-113) appeared concentrated in the internal capsule. These axons extended predominantly through the caudal divisions of the bed nuclei of the terminal stria (BST) (**Fig. 7A, B**). ILA projections in the BST contained numerous boutons and traveled through the interfascicular (BSTif), the transverse (BSTtr) and the ventral (BSTv) nuclei of the BST. In contrast, the principal nucleus (BSTpr) was devoid of axons in its dorsal half and contained some labeled axons in the ventral part for both cases.

A moderate density of vertically oriented fibers was also observed diverging from the internal capsule (**Fig. 7A**). This fiber group appeared to pass through the BST and traverse the innominate substance (SI) to reach the rostral parts of the amygdala; a fibers-of-passage interpretation for this group is supported by the general lack of axonal boutons and branching (**Fig. 7A–D**). Caudal to this group, a higher density of similarly oriented fibers was observed in a lateral part of the ventral zone of the anterior LHA region (LHAav) (**Fig. 7B–E**). Unlike the SI fiber group, ILA axons in the LHAav fiber group, particularly those lateral to the supraoptic nucleus (SO), were highly branched and contained a moderate density of boutons.

Although the fiber trajectories are less clear, the internal capsule-derived ILA axons appear to give rise to terminal fields within certain midline diencephalic structures. The paratenial (PT), the perireuniens (PR) and the reuniens (RE) clearly receive the densest ILA projections among the thalamic nuclei (**Fig. 7A–I**). PHA-L label in the PT appeared as meandering, thick axons which were covered with boutons (**Fig. 7A–C**). Medially, the paraventricular nucleus of the thalamus (PVT) received sparse ILA axons, which were oriented vertically and formed clear boutons (**Fig. 7A–C**). This dorsal fiber group continued ventrally through the anteromedial nucleus of the thalamus (AM) and into the RE. ILA projections were detected in low to moderate densities throughout the RE except for a few ventral structures which received heavy projections. Immunodetected axons targeted preferentially the ventral parts of the RE to include the ventral (REv) and lateral (REl) parts of the rostral division as well as the posterior (REcp) and dorsal (REcd) parts of the caudal

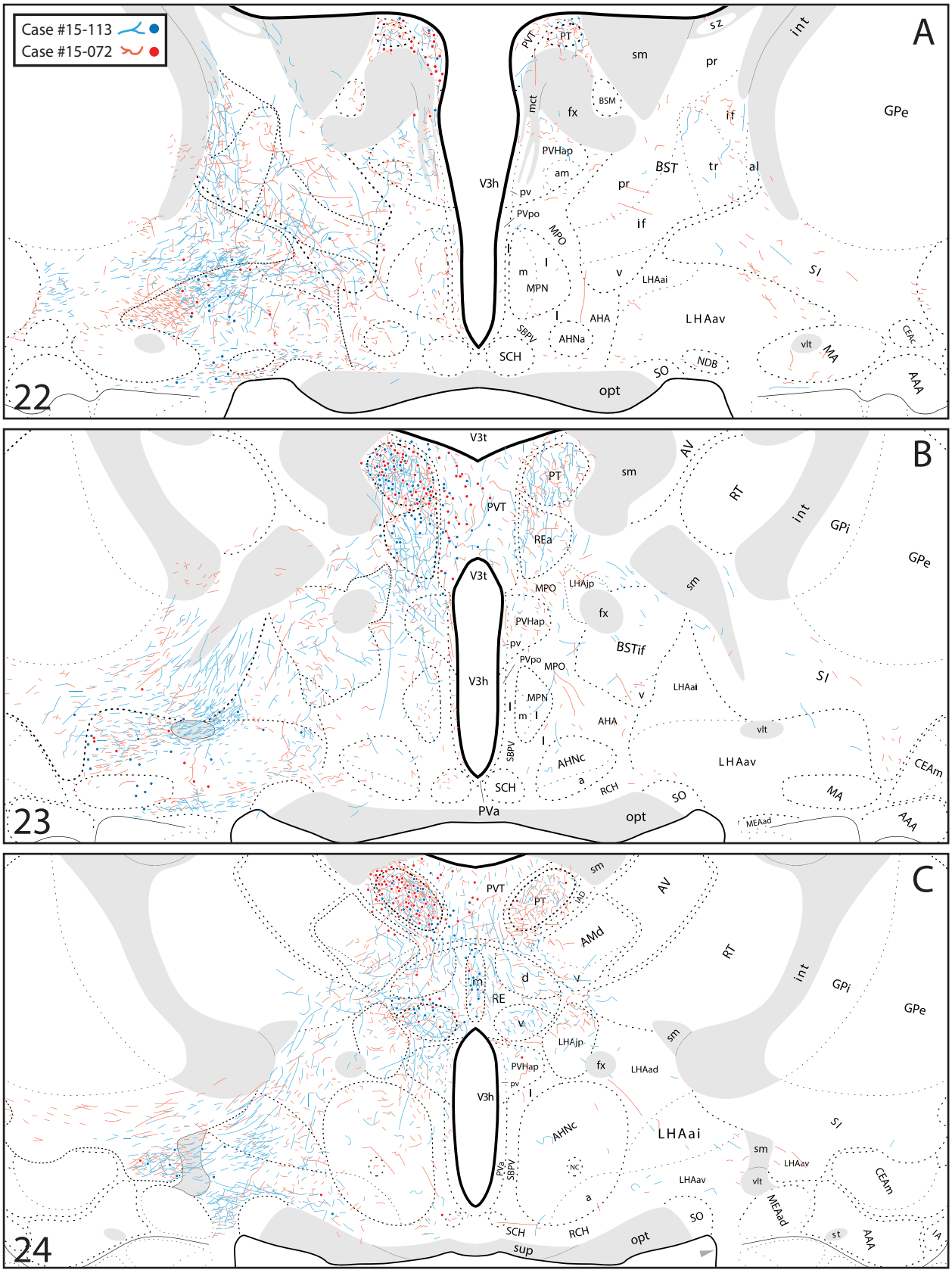
Case #15-113
Case #15-072
A
22
PVT
PT
sm
sz
int
pr
mct
fx
BSM
if
GPe
PVHap
am
BST
tr
al
V3h
pv
PVpo
MPO
l
m
MPN
v
LHAai
SI
AHA
LHAav
SBPV
AHNa
SCH
NDB
vlt
MA
CEAc
SO
opt
AAA
B
23
V3t
AV
RT
GPi
REa
LHAjp
BSTif
AHNc
a
RCH
PVa
MEAad
CEAm
C
24
AMd
d
RE
LHAad
NC
sup
st
IA

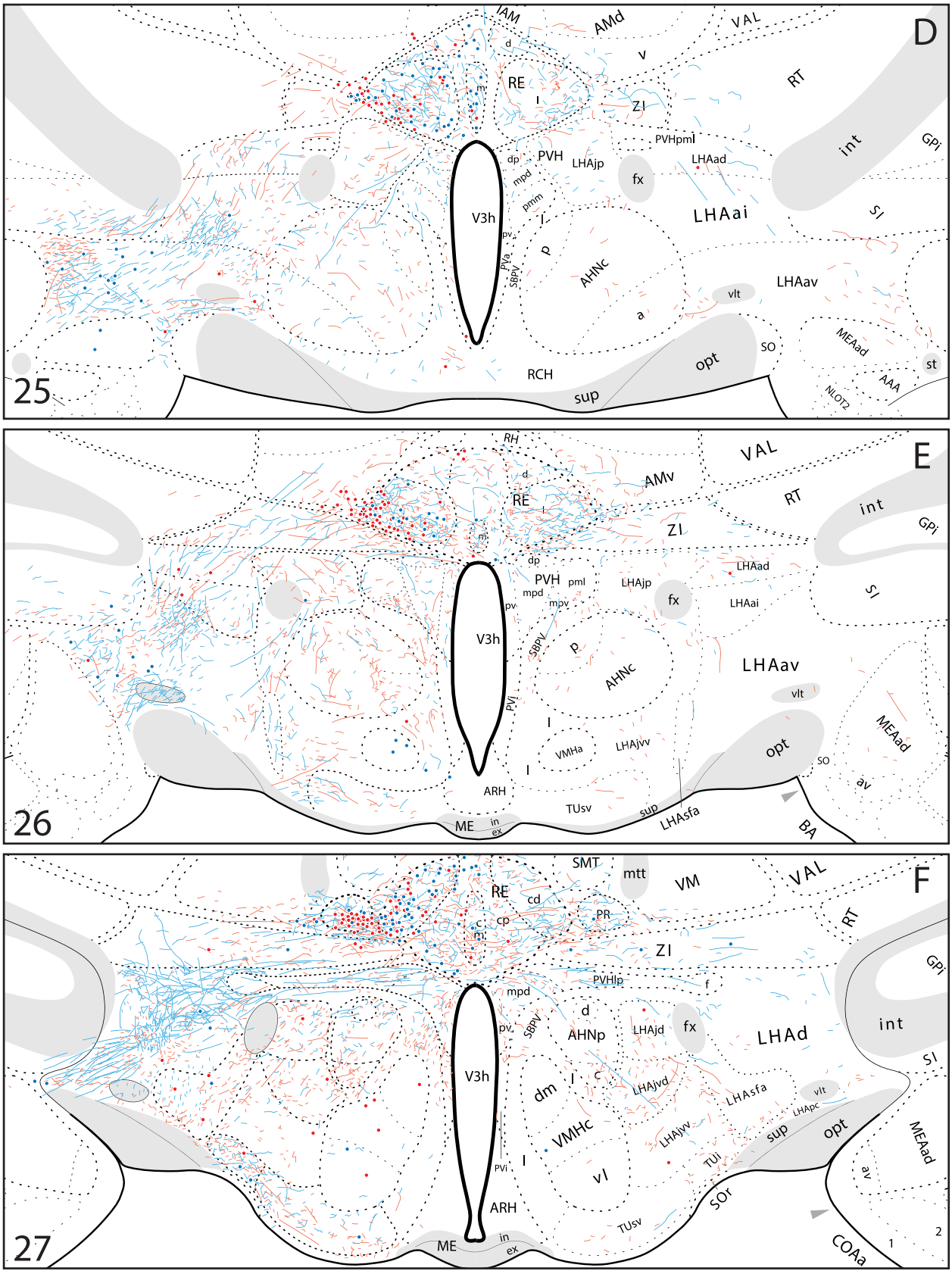
D
25
IAM
AMd
VAL
RE
ZI
RT
int
GPi
PVHpml
dp
PVH
LHAjp
LHAad
fx
mpd
pmm
V3h
LHAai
SI
pv
PVa
SBPV
p
AHNc
LHAav
vlt
a
SO
opt
MEAad
st
RCH
sup
AAA
NLOT2
E
26
RH
AMv
VAL
RE
RT
int
GPi
ZI
dp
PVH
pml
LHAjp
LHAad
mpd
mpv
fx
LHAai
SI
pv
V3h
SBPV
p
AHNc
LHAav
vlt
PVi
VMHa
LHAjvv
opt
MEAad
SO
av
ARH
TUsv
sup
LHAsfa
ME
in
ex
BA
F
27
SMT
mtt
VM
VAL
RE
cd
PR
cp
RT
GPi
ZI
PVHlp
f
mpd
d
AHNp
LHAjd
fx
LHAd
int
SI
pv
SBPV
V3h
dm
LHAjvd
LHAsfa
vlt
LHApc
VMHc
LHAjvv
sup
opt
MEAad
TUi
av
PVi
vl
ARH
SOr
TUsv
ME
in
ex
COAa
1
2

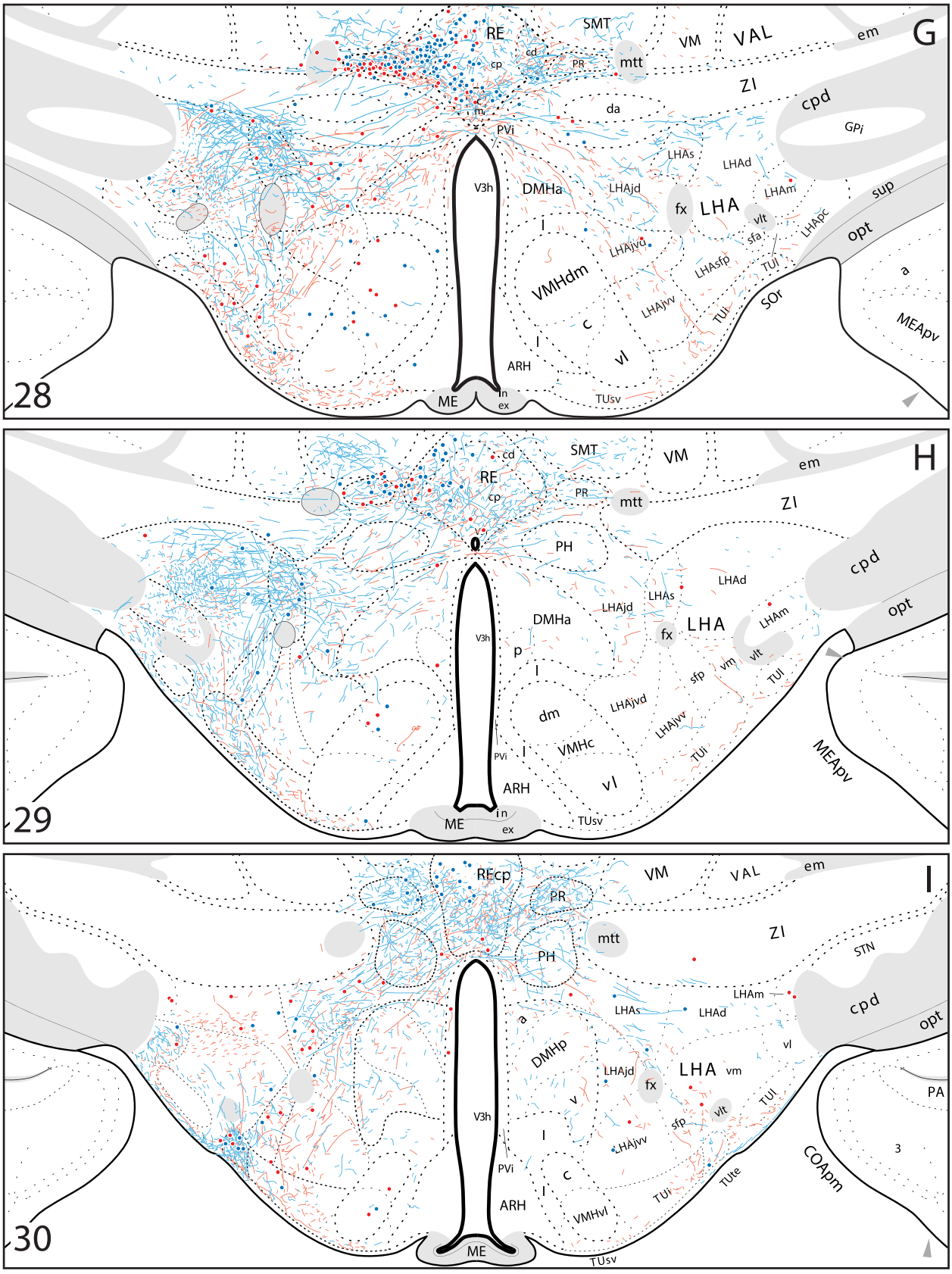
G
RE
SMT
VM
VAL
em
cd
cp
PR
mtt
ZI
cpd
da
mt
PVi
GPi
LHAs
LHAd
V3h
DMHa
LHAjd
fx
LHA
LHAm
sup
opt
vlt
sfa
LHApc
LHAjvd
LHAstp
TUl
VMHdm
LHAjvv
TUi
SOr
a
MEApv
c
l
vl
ARH
28
ME
in
ex
TUsv
H
cd
SMT
VM
em
RE
cp
PR
mtt
ZI
PH
cpd
LHAd
LHAs
opt
LHAjd
DMHa
LHAm
V3h
fx
LHA
p
l
vm
vlt
sfp
TUl
dm
LHAjvd
LHAjvv
PVi
VMHc
TUi
MEApv
ARH
vl
29
ME
in
ex
TUsv
I
REcp
VM
VAL
em
PR
mtt
ZI
STN
PH
LHAm
cpd
LHAs
LHAd
opt
a
DMHp
vl
LHAjd
fx
LHA
vm
PA
TUl
v
V3h
sfp
vlt
l
LHAjvv
3
PVi
c
COApm
TUi
TUte
ARH
VMHvl
30
ME
TUsv

Fig. 7 (previous three pages). Maps of ILA connections to the LHA and nearby structures. PHA-L-labeled axons are drawn as colored lines and individual CTb-backfilled cells are represented as colored dots. The color coding scheme is represented on the panel at the top left of Panel A. Injection site locations for these maps are shown in Figs. 5 and 6. Data are plotted onto reference atlas plates from Swanson (2004). Plates are arranged from rostral to caudal and the numbers on the bottom left of each panel denote atlas levels.

---

division (**Fig. 7C–I**). Towards the caudal end of the RE, PHA-L label in case #15-113 was also detected in the ventral part of the submedial thalamic nucleus (**Fig. 7G–I**). Contralateral ILA projections to these midline thalamic nuclei were also observed in lesser densities (**Fig. 7A–I**).

Caudal to the BST, ILA axons were found in lesser densities and with fewer boutons. Low densities of axons leaving the RE were detected in the juxtaparaventricular (LHAjp) and anterior (LHAa) regions of the LHA (**Fig. 7A–E**). Fewer axons were observed throughout the PVH; these took the appearance of axons en passant. Ventral to the LHAjp, the anterior hypothalamic nucleus (AHN) also received low density ILA innervation. Notably, the adjacent ventromedial hypothalamic nucleus (VMH) was devoid of ILA projections throughout its rostrocaudal extent.

ILA efferents to the LHA did not arrive exclusively through the internal capsule. A significant proportion of axons also branched from the medial forebrain bundle (MFB); these appeared as discrete clusters of caudally oriented axons in the lateral parts of the LHA. In case #15-113, MFB axons are seen in the boundary between the intermediate zone (LHAai) and the LHAav (**Fig. 7A–E**). Remarkably, MFB axons in the dorsal region (LHAd) appeared to branch extensively and form boutons of passage (**Fig. 7F–I**). This contrasted with rostral parts of the same bundle which only took the appearance of passing fibers (*compare* **Fig. 7E, F**).

Labeled axons oriented towards the amygdala were observed in the MFB within the LHAd as in the capsular axonal group (**Fig. 7F**). Most of the MFB axons extended through the LHAd and gave rise to terminal fields in the suprafornical region (LHAs) (**Fig. 7F–H**). ILA axons in the LHAs and LHAd were highly branched and produced a moderate density of boutons (**Fig. 8**). A smaller proportion of these fibers terminated in the juxtaparaventricular region (LHAjp). These LHA subdivisions also received minor contralateral innervation. Decussating axons from the LHAd passed through the zona incerta (ZI), the lateral (PVHlp) and medial parvicellular (PVHmpd) parts

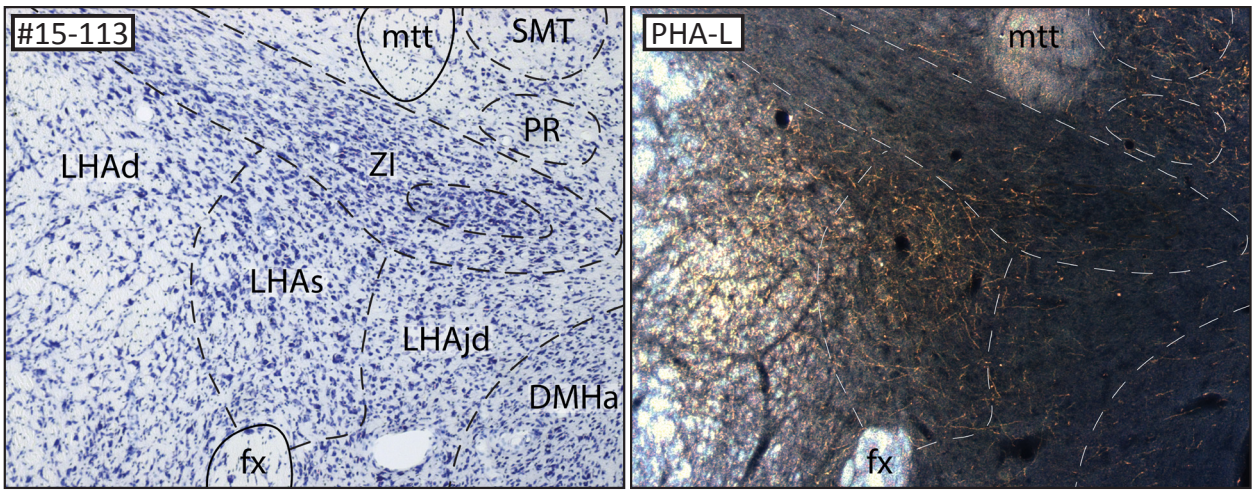

Fig. 8. Representative photomicrographs showing PHA-L labeling in the dorsal LHA. (Left) Adjacent thionin-stained section showing parcellations of structures surrounding the LHAs. Regional boundaries are shown as dashed lines, white matter tracts are outlined with bold lines. (Right) Darkfield photomicrograph showing immunoperoxidase staining for PHA-L in the LHAd and the LHAs.

---

of the paraventricular hypothalamic nucleus (PVH) to cross over at the ventral region of the RE (**Fig. 7F–I**).

ILA projections descending from the MFB also target, in low to moderate densities, the ventral LHA structures. A low density of passing fibers crossed the subfornical region (LHAsf) to innervate the tuberal nucleus (TU). PHA-L-positive axons from both injections were found in the intermediate (TUi) and terete (TUte) subdivisions of the tuberal nucleus (**Figs. 7F–I; Fig. 9**). Interestingly, efferents from injection #15-113, and not from case #15-072, produced dense terminals in the TUte (**Fig. 7I**). We also note a contrasting paucity of axons in the adjacent lateral part (TUl), which was skirted by axons from the lateral (LHAvl) and medial (LHAvm) zones of the ventral LHA region.

III.2.2. Aim 2b: Afferent connections of the ILA (CTb retrograde tracing). In general, the spread of CTb at the injection sites was concentrated in the layer 3/5 boundary and tracer spread was minimal or undetected in the deepest and most superficial layers (**Fig. 7**). While it is important to interpret these results as partially representative of ILA afferents, patterns nonetheless begin to emerge when multiple injections are considered. A detailed account of the regional distributions

of CTb-labeled cells will be given in a presentation order that reflects the developmental sequence specified by Swanson (2015): Rostral regions will be described before caudal ones, then medial before lateral, and then ventral before dorsal.

Immunodetected CTb in the cerebral hemispheres was found almost exclusively in cortical structures while low numbers were also detected in the striatum and the pallidum. Nonetheless, some retrograde label was found within ventral pallidal regions. CTb-positive cells were found in parts of the SI, typically where PHA-L-filled axons were present (**Fig. 7A, B, E**). A small cluster of ILA-projecting cells also populated the magnocellular nucleus (MA) of case #15-113 (**Fig. 7B**). Only one cell was noted in the BSTif (**Fig. 7A**). In contrast, strong bilateral connectivity was observed in certain amygdalar nuclei and the hippocampal formation (*not shown*).

Diencephalic projections to the CNG originated mostly from the thalamus; however, the spatial resolution granted by the current parcellation strategy warrants a detailed examination of ILA afferents from the more sparsely connected hypothalamus. The current nomenclature system divides the hypothalamus into three zones: The periventricular, the medial and the lateral zones (Nauta and Haymaker, 1969; Swanson, 2016).

CTb injections into the ILA did not produce many labeled cells in the periventricular zone. A smattering of retrogradely labeled cells were found near the third ventricle; these were distributed

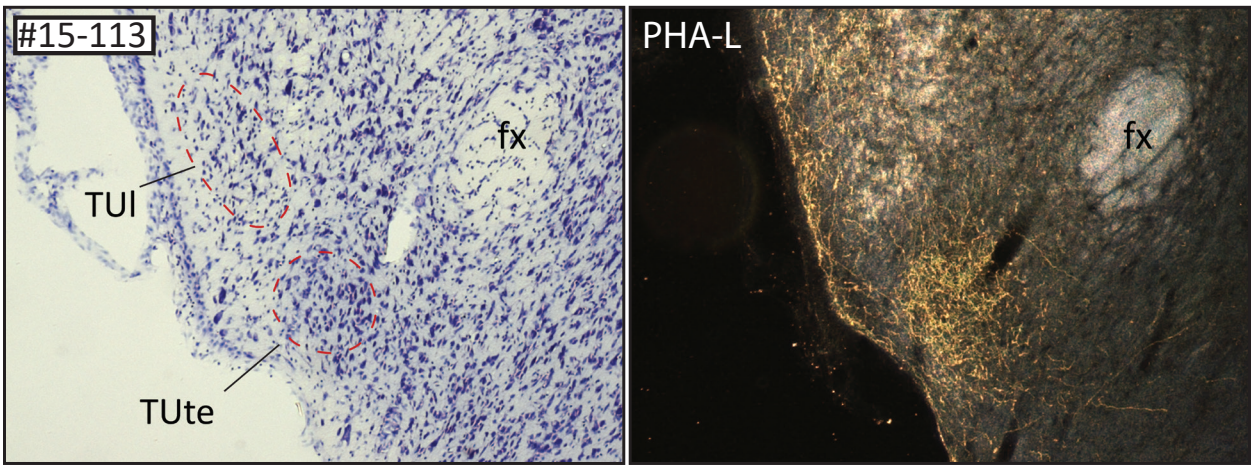

Fig. 9. Representative photomicrographs showing PHA-L labeling in a ventrolateral part of the caudal LHA. (Left) Adjacent thionin-stained section showing parcellations for distinct TU subdivisions, boundaries are denoted with dashed red lines. (Right) Darkfield photomicrograph showing PHA-L labeling in the TUte detected using an immunoperoxidase reaction.

among the internuclear area (I), the subparaventricular zone (SBPV), the arcuate nucleus (ARH), the intermediate (PVi) and anterior (PVa) parts of the periventricular hypothalamic nucleus (**Fig. 7D–I**). CTb-filled cells in the paraventricular hypothalamic nucleus were restricted to the anterior parvicellular part (PVHap) (**Fig. 7A, C**). ILA-projecting neurons were detected in the dorsomedial nucleus (DMH) for case #15-072 (**Fig. 7G, H**) The posterior nucleus contained the largest population of CTb-labeled cells in the periventricular zone (**Fig. 7K**).

ILA afferents from the medial zone were limited to the ventromedial hypothalamic nucleus (VMH). Labeled cells were present throughout the rostrocaudal extent of the VMH, which as previously noted had a marked absence of PHA-L-labeled axons (**Fig. 7E–I**).

The hypothalamic lateral zone (LZ) contained most of the hypothalamic CNG-projecting neurons labeled by our CTb injections. Starting rostrally, a few CTb-labeled cells were detected in the retrochiasmatic area (RCH) (**Fig. 7C, D**). Retrogradely labeled cells in the anterior region, predominantly from case #15-113, were mostly contained in the LHAav (**Fig. 7A–E**). The dorsally adjacent LHAai and dorsal LHAad contained comparatively fewer labeled cells. Labeled neurons were concentrated in the ventrolateral LHAav, particularly where anterogradely labeled axons were also found.

A medial tier of the LHA, which includes subdivisions medial to the fornix, contained less CTb-labeled neurons than the anterior group. Only one CTb-labeled neuron was found in the LHAjp and a few were scattered throughout the rostrocaudal extent of the LHAjvd and LHAjvv (**Fig. 7E–I**). Caudal to the LHAjp, a modest density of retrogradely filled neurons was found in the LHAjd (**Fig. 7F, G**). These labeling patterns were observed bilateral to some extent and most labeled neurons were seen in case #15-113.

Retrograde labeling was consistently present in the perifornical tier. CTb-positive neurons in the LHAs, the LHAsfa and the LHAsfp were present throughout each subdivision's rostrocaudal extent for both injection cases (**Fig. 7F–I**).

CTb-filled cells in the lateral tier of the LHA were present throughout its rostrocaudal extent but were slightly denser in its caudal parts. ILA-targeting neurons in the tuberal nucleus

were largely distributed between the TUi and the TUte, the latter containing a small cluster of labeled cells (**Fig. 7F–I**). In contrast, the TUsv and TUl did not contain CTb-labeled cells. More laterally, some CTb-positive cells were observed in the LHAvm, the LHAvl and the LHAm (**Fig. 7F–I**). Dorsally, the LHAd contained a moderate density of labeled cells.

ILA connectivity was observed mostly with midline thalamic nuclei. The PT contained the highest density of labeled cells through its rostrocaudal extent (**Fig. 7A–C**). A somewhat lower density of CTb labeling was distributed more medially in the PVT (**Fig. 7A–C**). Retrograde labeling was present throughout the RE but was distributed in certain ventral subdivisions. In the rostral division, moderate densities of CTb labeling were found in the median (REm), the anterior (REa), the lateral (REl) and the ventral (REv) parts (**Fig. 7B–E**). Notably, the dense retrograde labeling from both injections appeared to organize into discrete clusters in the caudal division of the RE. CTb labeling from case #15-113 was concentrated in the dorsal part (REcd) whereas case #15-072 predominantly labeled the PR (**Fig. 7F–H**).

Chapter IV: Discussion

IV.1: Chemoarchitecture of CNG interneurons

Aim 1 of this study was to produce high-spatial resolution maps to support a robust account of CNG connectional architecture with peptidergic inputs from neurons concentrated in the hypothalamus. First, immunohistochemistry was combined with a cytoarchitecture-based mapping strategy to examine the distributions of certain GABAergic interneurons and H/O-ir axons in the CNG. This was followed, in *Aim 2*, by a detailed account of the macroconnections between the ILA and the hypothalamus. Although these datasets are inherently irreconcilable, the spatial framework used here greatly facilitates multimodal data integration with one degree of abstraction (Khan, 2013). Technical innovations, specifically those involving promoter-targeting gene manipulations, have rekindled efforts to understand the functional dynamics of GABAergic CNG interneurons (Pinto and Dan, 2015; Kim, 2016). Investigations into CNG chemoarchitecture typically focused on the general distributions of single peptides, whereas here they were examined simultaneously within a framework that allows multimodal data integration. We will discuss the observed chemoarchitectural features prior to a discussion of their functional implications.

CB and PV cellular distributions throughout the brain are best left to the tour de force contribution of Celio (1990). Reported CB and PV immunoreactivity occurred as overlapping fields in the dorsal CNG, which is somewhat at odds with CB distributions shown here (**Fig. 2**). The tendency for PV label to be densest in the dorsal CNG is supported by quantitative work and was also seen in mice (Gabbott et al., 1997; Van De Werd et al., 2010). CB aggregation in superficial CNG layers was also noted in the work mentioned above but the observation that CB density is predominant in the ILA of caudal levels is not in agreement with other reports (Celio, 1990; Gabbott et al., 1997; Van De Werd and Uylings, 2008). This discrepancy could have resulted from two differences. First, the use of curved boundaries (**Fig. 1A**), as opposed to straight lines, by Swanson (2004) accounts for some of the interlaminar differences. It is likely that differences with the quantitative data (Gabbott et al., 1997) resulted from the sampling range, note that CB labeling in rostral parts of the ILA are hardly distinguishable from CNG areas of the same level

(**Fig. 2**). Laminar segregation described here for PV and CB in the caudal ILA offer an interesting extension to the initial observations by Celio (1990), that the two peptides tend to occupy different but complementary brain regions. SS cell distributions appeared uniformly distributed throughout the CNG and, unlike PV and CB, populated layer 6. Less work has gone towards establish the distribution of SS in the CNG (Johansson et al., 1984).

IV.1.1: Cellular targets of H/O axons in the CNG. Projections from hypothalamic H/O neurons to the CNG have been well-described (Peyron et al., 1998; Nambu et al., 1999; Baldo et al., 2003; Jin et al., 2016). Although H/O immunoreactivity in the cortex is less robust than in subcortical structures (Peyron et al., 1998), the distributions shown here suggest certain organizational trends. H/O-ir fibers appeared to preferentially target the ventral CNG, especially in more caudal parts. Baldo (2003) recognized slightly denser H/O labeling in the ILA but the trend has yet to be quantitatively addressed. Recent work has partially supported this by showing increased fiber length and orexin receptor 1 expression in the caudal CNG (Jin et al., 2016). Nevertheless, more work must be done to understand the contributions of H/O to cortical functions.

IV.2: CNG connections with the hypothalamus

Input and output connections of the CNG are among the most intensely studied brain regions. CNG connectivity is understood through decades of research involving pathway tracing using various methodologies (Nauta, 1964; Domesick, 1969; Krettek and Price, 1977; Sesack et al., 1989; Hoover and Vertes, 2007; Negishi et al., 2015). Connections described in the present study are largely complemented by the published and, in one case, unpublished literature (Brittain, 1988).

Descending ILA projections to the striatum and pallidum produced terminal fields in ventral structures. These connections were almost exclusively unilateral given a paucity of retrograde label in the BSTif and SI (**Fig. 7**). ILA projections to the BST have been previously described (Vertes, 2004) but the relative absence of PHAL label in the BSTpr has not been explicitly noted despite being represented (Vertes, 2004). This is interesting given that BSTpr projections produce terminal fields in regions which scarcely receive ILA projections, possibly suggesting a participation in

non-overlapping networks (Dong and Swanson, 2004).

ILA connections with the various hypothalamic nuclei shown here are in agreement with previous work (Britain, 1988; Hurley et al., 1991; Vertes, 2004). These easily distinguishable cell groups form the so-called rostral "behavior control column," (BCC) which is critical for the coordinated expression of various behaviors (Swanson, 2000). Descending ILA projections to members of the BCC could offer a direct pathway for influencing behavioral outcomes. Low-to-moderate densities of ILA projections to the AHN, which are involved in coordinating defensive-aggressive behavior (Hilton and Redfern, 1986). Some ILA axons detected in the MPN, a region associated with reproductive behaviors, were also retrogradely confirmed (Simerly and Swanson, 1986). ILA afferents from the VMH shown here conflicted with results from another retrograde study (Hoover and Vertes, 2007); however, anterograde injections into the VMH clearly showed labeling in the CNG (Canteras et al., 1994). Although ILA inputs to the BCC are in some cases meager, the ILA can indirectly shape BCC activity by engaging certain upstream striatal and pallidal structures (Swanson, 2000).

IV.2.1: ILA connections with the LHA. The LHA is a vast and poorly understood structure. Its neuroanatomical investigation is complicated by the networks of collateral and passing fibers diverging from the MFB and other white matter tracts (see introduction from Hahn and Swanson, 2010). Compared to its neighboring structures, the LHA is less amenable to subdivision based on cytoarchitecture; LHA cellular organization is relatively homogeneous and lacks obvious cell aggregations which could be classified as nuclei. Nonetheless, the LHA parcellation scheme used here takes advantage of subtle but stable cytoarchitectonic features to use as provisional subdivisions (Swanson, 2004; Swanson et al., 2005).

Recent work has undertaken the non-trivial task of establishing the connections of these LHA subdivisions by using small injections of tracers. So far, this effort has achieved a coverage of seven out of 25 LHA subregions (Goto, 2005; Hahn and Swanson, 2010; Hahn and Swanson, 2012; Hahn and Swanson, 2015). Anterograde and retrograde transport shown here for the ILA are congruent with these reports except for retrograde labeling in the LHAs. Bidirectional ILA-LHAs

connectivity is reported here throughout the rostrocaudal extent of the LHAs. This is at odds with tracer injections into the LHAs which reported a high density of retrograde, but not anterograde labeling, in the ILA (Hahn and Swanson, 2010); moreover, fluorogold injections into the ILA also reported no retrograde transport in the vicinity of the LHAs (Hoover and Vertes, 2007).

IV.3: Functional significance within the context of ingestive behaviors

CNG activity is thought to support the associative learning of—and the ability to act on—food-related cues (Petrovich, 2011). Indeed, Pavlovian conditioning depends on an intact CNG to trigger feeding in sated rats (Petrovich et al., 2007). Recent work has also shown that sated rats could be induced to overeat by infusing μ-opioid receptor agonists into the ventral CNG (Mena et al., 2011). Overeating driven by associative learning and the endocannabinoid system clearly engage ventral CNG structures, but the degree to which they share neural substrates is not well-understood. Both models have demonstrated selective Fos induction in H/O-ir neurons dorsal to the fornix at the level of the DMH (Petrovich et al., 2012; Mena et al., 2013). This region likely corresponds to the LHAs, which contains a large proportion of hypothalamic H/O neurons (Swanson et al., 2005; Hahn, 2010). Here we found that ILA projections gave rise to terminal fields in the LHAs (**Fig. 7H**), and these projections were demonstrated to make appositions onto H/O neurons (Yoshida et al., 2005)

Future investigations, for example, using optogenetics, are needed to determine whether monosynaptic ILA projections to the LHA are sufficient to elicit feeding. In addition to providing clear targets for optogenetic probes, the present study also demonstrates that ILA-originating axons in the LHA tend to distribute widely and produce many collaterals. However, a direct ILA-LHA pathway does not preclude the contributions of indirect pathways through intermediate relays. Such relays between the CNG and the hypothalamus have been identified at a structural level and are believed to influence functions by relaying information to brain regions which do not receive direct CNG inputs (Vertes, 2002; Radley et al., 2009; Thompson and Swanson, 2010).

IV.4. Concluding remarks

In this study, we demonstrated the effectiveness of a cytoarchitecture-based mapping approach. Extensive analysis of CNG chemical and connectional architecture revealed novel targets for functional studies. These findings also contribute to a community effort to build a neuroanatomical connectome of the rat brain (Bota et al., 2015). Beyond connectomes, atlas space also serves as an integrative platform for multiscale datasets ranging from behavioral to proteomic data (Khan, 2013).

Literature Cited

1. Baldo BA, Daniel RA, Berridge CW, Kelley AE. 2003. Overlapping distributions of orexin/hypocretin- and dopamine-β-hydroxylase immunoreactive fibers in rat brain regions mediating arousal, motivation, and stress. *J Comp Neurol* 464:220–237.

2. Balfour ME, Brown JL, Yu L, Coolen LM. 2006. Potential contributions of efferents from medial prefrontal cortex to neural activation following sexual behavior in the male rat. *Neurosci* 137:1259–1276.

3. Berthoud HR, Münzberg H. 2011. The lateral hypothalamus as integrator of metabolic and environmental needs: from electrical self-stimulation to opto-genetics. *Physiol Behav* 104(1):29–39.

4. Blanchard TC, Hayden BY. 2014. Neurons in dorsal anterior cingulate cortex signal postdecisional variables in a foraging task. *J Neurosci* 34(2):646–655.

5. Bota M, Sporns O, Swanson LW. 2015. Architecture of the cerebral cortical association connectome underlying cognition. *Proc Natl Acad Sci U S A* 112:E2093–101.

6. Brittain DA. 1988. *The efferent connections of the infralimbic cortex in the rat.* Doctoral dissertation. University of California, San Diego.

7. Brodmann K. Vergleichende lokalisationslehre der Ggoßhirnrinde in ihren prinzipien dargestellt auf grund des zellenbaues (Barth, Leipzig, 1909); English translation available in Garey, L. J. *Brodmann's Localization in the Cerebral Cortex* (Smith Gordon, London, 1994).

8. Buzsáki G, Wang XJ. 2012. Mechanisms of gamma oscillations. *Annu Rev Neurosci* 35:203–225.

9. Canteras NS, Simerly RB, Swanson LW. 1994. Organization of projections from the ventromedial nucleus of the hypothalamus: a *Phaseolus vulgaris*-leucoagglutinin study in the rat. *J Comp Neurol* 348:41–79.

10. Castro DC, Berridge KC. 2014. Opioid hedonic hotspot in nucleus accumbens shell: mu, delta, and kappa maps for enhancement of sweetness “liking” and “wanting”. *J Neurosci* 34(12):4239–4250.

11. Celio MR. 1990. Calbindin D-28k and parvalbumin in the rat nervous system. *Neurosci* 35(2):375–475.

12. Cole S, Hobin MP, Petrovich GD. 2015. Appetitive associative learning recruits a distinct network with cortical, striatal, and hypothalamic regions. *Neurosci* 286:187–202.

13. Cvetkovic V, Brischoux F, Griffond B, Bernard G, Jacquemard C, Fellman D, Risold PY. 2003. Evidence of melanin-concentrating hormone-containing neurons supplying both cortical and neuroendocrine projections. *Neurosci* 116:31–35.

14. de Lecea L, Kilduff TS, Peyron C, Gao XB, Foye PE, Danielson PE, Fukuhara C, Battenberg ELF, Gautvik VT, Bartlett II FS, Frankel WN, van den Pol AN, Bloom FE, Gautvik KM, Sutcliffe JG. 1998. The hypocretins: hypothalamus-specific peptides with neuroexcitatory activity. *Proc Nat Acad Sci U S A* 95(1):322–327.

15. Delgado JK, Anand BK. 1953. Increase of food intake induced by electrical stimulation of the lateral hypothalamus. *Amer J Physiol* 172(1), 162–168.

16. Domesick VB. 1969. Projections from the cingulate cortex in the rat. *Brain Res* 12:296–320.

17. Euston DR, Gruber AJ, McNaughton BL. 2012. The role of medial prefrontal cortex in memory and decision making. *Neuron* 76: 1057–1070.

18. Fujisawa S, Amarasingham A, Harrison MT, Buzsáki G. Behavior-dependent short-term assembly dynamics in the medial prefrontal cortex. *Nat Neurosci* 11:823–833.

19. Gabbott PLA, Warner TA, Jays PRL, Salway P, Busby SJ. 2005. Prefrontal cortex in the rat: projections to subcortical autonomic, motor, and limbic centers. *J Comp Neurol* 492:147–177.

20. Gabbott PLA,Dickie BGM, Vaid RR, Headlam AJN, Bacon SJ. 1997. Local-circuit neurones in the medial prefrontal cortex (areas 25, 32 and 24b) in the rat: morphology and quantitative distribution. *J Comp Neurol* 377:465–499.

21. Gerfen CR, Sawchenko PE. 1984. An anterograde neuroanatomical tract tracing method that shows the detailed morphology of neurons, their axons and terminals: immunohistochemical localization of an axonally transported plant lectin, *Phaseolus vulgaris* leucoagglutinin (PHA-L). *Brain Res* 290:219–238.

22. Goto M, Canteras NS, Burns G, Swanson LW. 2005. Projections from the subfornical region of the lateral hypothalamic area. *J Comp Neurol* 493:412–438.

23. Grossman SP. 1960. Eating or drinking elicited by direct adrenergic or cholinergic stimulation of hypothalamus. *Science* 132(3422):301–302.

24. Hahn JD. 2010. Comparison of melanin-concentrating hormone and hypocretin/orexin peptide expression patterns in a current parceling scheme of the lateral hypothalamic zone. *Neurosci Lett* 468:12–17.

25. Hahn JD, Swanson LW. 2010. Distinct patterns of neuronal inputs and outputs of the juxtaparaventricular and suprafornical regions of the lateral hypothalamic area in the male rat. *Brain Res Rev* 64:14–103.

26. Hahn JD, Swanson LW. 2012. Connections of the lateral hypothalamic area juxtadorsomedial region in the male rat. *J Comp Neurol* 520:1831–1890.

27. Hahn JD, Swanson LW. 2015. Connections of the juxtaventromedial region of the lateral hypothalamic area in the male rat. *Front Syst Neurosci* 9:66.

28. He C, Chen QH, Ye JN, Li C, Yang L, Zhang J, Xia JX, Hu ZA. 2015. Functional inactivation of hypocretin 1 receptors in the medial prefrontal cortex affects the pyramidal neuron activity and gamma oscillations: an *in vivo* multiple-channel single-unit recording study. *Neurosci*

297:1–10.

29. Heidbreder CA, Groenewegen HJ. 2003. The medial prefrontal cortex in the rat: evidence for a dorso-ventral distinction based upon functional and anatomical characteristics. *Neurosci Biobehav Rev* 27:555–579.

30. Hilton SM, Redfern WS. 1986. A search for brainstem cell groups integrating the defense reaction in the rat. *J Physiol* 378:213–22.

31. Hoebel BG, Teitelbaum P. 1962. Hypothalamic control of feeding and self-stimulation. *Science* 135:375–377.

32. Hoover WB, Vertes RP. 2007. Anatomical analysis of afferent projections to the medial prefrontal cortex in the rat. *Brain Struct Funct* 212:149–179.

33. Horvath TL, Peyron C, Diano S, Ivanov A, Aston-Jones G, Kilduff TS, van den Pol AN. 1999. Hypocretin (orexin) activation and synaptic innervation of the locus coeruleus noradrenergic system. *J Comp Neurol* 415(2):145–159.

34. Hurley KM, Herbert H, Moga MM, Saper CB. 1991. Efferent projections of the infralimbic cortex of the rat. *J Comp Neurol* 308:249–276.

35. Jennings JH, Rizzi G, Stamatakis AM, Ung RL, Stuber GD. 2013. The inhibitory circuit architecture of the lateral hypothalamus orchestrates feeding. *Science* 341:1517–1521.

36. Jin J, Chen Q, Qiao Q, Yang L, Xiong J, Xia J, Hu Z, Chen F. 2016. Orexin neurons in the lateral hypothalamus project to medial prefrontal cortex with a rostro-caudal gradient. *Neurosci Lett* 621:9–14.

37. Johansson O, Hökfelt T, Elde RP. 1984. Immunohistochemical distribution of somatostatin-like immunoreactivity in the central nervous system of the adult rat. *Neurosci* 13(2):265–339.

38. Khan AM. 2013. Controlling feeding behavior by chemical or gene-directed targeting in the

brain: what's so spatial about our methods? *Front Syst Neurosci* 7:1–49.

39. Kim H, Ährlund-Richter S, Wang Xinming, Deisseroth K, Carlén M. 2016. Prefrontal parvalbumin neurons in control of attention. *Cell* 164:208–218.

40. Klausberger T, Somgyi P. 2008. Neuron diversity and temporal dynamics: the unity of hippocampal circuit operations. *Science* 321:53–57.

41. Krettek JE, Price JL. 1977. The cortical projections of the mediodorsal nucleus and adjacent thalamic nuclei in the rat. *J Comp Neurol* 171:157–192.

42. Land BB, Narayanan NS, Liu R, Gianessi CA, Brayton CE, Grimaldi DM, Sarhan M, Guarnieri DJ, Deisseroth K, Aghajanian GK, DiLeone RJ. 2014. Medial prefrontal D1 dopamine neurons control food intake. *Nat Neurosci* 17:248–253.

43. Lodato S, Arlotta P. 2015. Generating neuronal diversity in the mammalian cerebral cortex. *Annu Rev Cell Dev Biol* 31:699–720.

44. Luppi PH, Fort P, Jouvet M. 1990. Iontophoretic application of unconjugated cholera toxin B subunit (CTb) combined with immunohistochemistry of neurochemical substances: a method for transmitter identification of retrogradely labeled neurons. *Brain Res* 534:209–224.

45. Mena JD, Sadeghian K, Baldo BA. 2011. Induction of hyperphagia and carbohydrate intake by μ-opioid receptor stimulation in circumscribed regions of frontal cortex. *J Neurosci* 31:3249–3260.

46. Mena JD, Selleck RA, Baldo BA. 2013. Mu-opioid stimulation in rat prefrontal cortex engages hypothalamic orexin/hypocretin-containing neurons, and reveals dissociable roles of nucleus accumbens and hypothalamus in cortically driven feeding. *J Neurosci* 33:18540–18552.

47. Merchant H, de Lafuente V, Peña-Ortega F, Larriva-Sahd J. 2012. Functional impact of interneuronal inhibition in the cerebral cortex of behaving animals. *Prog Neurobiol* 99:163–178.

48. Miller EK, Cohen JD. 2001. An integrative theory of prefrontal cortex function. *Annu Rev Neurosci* 24:167–202.

49. Monzon ME, de Barioglio SR. 1999. Response to novelty after i.c.v. injection of melanin-concentrating hormone in rats. *Physiol Behav* 67(5):813–817.

50. Monzon ME, de Souza MM, Izquierdo LA, Izquierdo I, Barros DM, de Barioglio SR. 1999. Melanin-concentrating hormone modifies memory retention in rats. *Peptides* 20:1517–1519.

51. Morgane PJ. 1961. Distinct "feeding" and "hunger motivating" systems in the lateral hypothalamus of the rat. *Science* 133:887–888.

52. Nambu T, Sakurai T, Mizukami K, Hosoya Y, Yanagisawa M, Goto K. 1999. Distribution of orexin neurons in the adult rat brain. *Brain Re*s 827:243–260.

53. Nauta WJH. 1964. "Some efferent connections of the prefrontal cortex in the monkey," in *The Frontal Granular Cortex and Behavior*, Warren JM, Akert K (eds.). McGraw Hill, NY. pp. 397–409.

54. Nauta WJH, Haymaker W. 1969. "Hypothalamic nuclei and fiber connections," in *The Hypothalamus*, Haymaker W, Anderson E and Nauta WJH (eds.). Illinois, IL: Charles C Thomas. pp. 136–209.

55. Negishi K, Hamdan J, Khan AM. 2015. Initial chemoarchitectural and connectional characterization of polymodal association cortical structures with the diencephalon: immunohistochemical and tract tracing studies in the adult male rat. Program No. 616.14. *2015 Neuroscience Meeting Planner*. Chicago, IL. Society for Neuroscience, 2015. Online.

56. O'Connor EC, Kremer Y, Lefort S, Harada M, Pascoli V, Rohner C, Luscher C. 2015. Accumbal D1R neurons projecting to lateral hypothalamus authorize feeding. *Neuron* 88: 1–12.

57. Olds J, Milner P. 1954. Positive reinforcement produced by electrical stimulation of septal area and other regions of rat brain. *J Comp Physiol Psych* 47:419–427.

58. Paxinos G, Watson C. 2014. Paxinos and Watson's *The Rat Brain in Stereotaxic Coordinates, 7th ed*. Elsevier Academic Press, San Diego.

59. Petrovich GD, Holland PC, Gallagher M. 2005. Amygdalar and prefrontal pathways to the lateral hypothalamus are activated by a learned cue that stimulates eating. *J Neurosci* 25:8295–8302.

60. Petrovich GD, Ross CA, Holland PC, Gallagher M. 2007. Medial prefrontal cortex is necessary for an appetitive contextual conditioned stimulus to promote eating in sated rats. *J Neurosci* 27:6436–6441.

61. Petrovich GD. 2011. Forebrain circuits and control of feeding by learned cues. *Neurobiol Learn Mem* 95:152–158.

62. Petrovich GD, Hobin MP, Reppucci CJ. 2012. Selective Fos induction in hypothalamic orexin/hypocretin, but not melanin-concentrating hormone neurons, by a learned food-cue that stimulates feeding in sated rats. *Neurosci* 224:70–80.

63. Peyron C, Tighe DK, van den Pol AN, de Lecea L, Heller HC, Sutcliffe JG, Kilduff TS. 1998. Neurons containing hypocretin (orexin) project to multiple neuronal systems. *J Neurosci* 18(23):9996–10015.

64. Pinto L, Dan Y. 2015. Cell-type-specific activity in prefrontal cortex during goal-directed behavior. *Neuron* 87:437–450.

65. Qu D, Ludwig DS, Gammeltoft S, Piper M, Pelleymounter MA, Cullen MJ, Mathes WF, Przypek J, Kanarek R, Maratos-Flier E. 1996. A role for melanin-concentrating hormone in the central regulation of feeding behavior. *Nature* 380:243–274.

66. Radley JJ, Gosselink KL, Sawchenko PE. 2009. A discrete GABAergic relay mediates medial prefrontal cortical inhibition of the neuroendocrine stress response. *J Neurosci* 29(22):7330–7340.

67. Rossi M, Choi SJ, O'Shea D, Miyoshi T, Ghatei MA, Bloom SR. 1997. Melanin-concentrating hormone acutely stimulates feeding, but chronic administration has no effect on body weight. *Endocrinol* 138(1):351–355.

68. Sakurai T. 1998. Orexins and orexin receptors: a family of hypothalamic neuropeptides and G protein-coupled receptors that regulate feeding behavior. *Cell* 92:573–585.

69. Schwarz C, Bolz J. 1991. Functional specificity of a long-range horizontal connection in cat visual cortex: a cross-correlation study. *J Neurosci* 11(10):2995–3007.

70. Sesack SR, Deutch AY, Roth RH, Bunney BS. 1989. Topographical organization of the efferent projections of the medial prefrontal cortex in the rat: an anterograde tract-tracing study with Phaseolus vulgaris leucoagglutinin. *J Comp Neurol* 290:213–242.

71. Simerly RB, Swanson LW. 1986. The organization of neural inputs to the medial preoptic nucleus of the rat. *J Comp Neurol* 246:312–342.

72. Swanson LW. 2000. Cerebral hemisphere regulation of motivated behavior. *Brain Res* 886:113–164.

73. Swanson LW. 2004. *Brain Maps: Structure of the Rat Brain, 3rd ed*. San Diego: Academic Press.

74. Swanson LW, Swanchez-Watts G, Watts AG. 2005. Comparison of melanin-concentrating hormone and hypocretin/orexin mRNA expression patterns in a new parceling scheme of the lateral hypothalamic zone. *Neurosci Lett* 387:80–84.

75. Swanson LW. 2015. *Neuroanatomical Terminology: A lexicon of classical origins and historical foundations*. Oxford: Oxford Univ Press.

76. Swanson LW, Lichtman JW. 2016. From Cajal to connectome. *Annu Rev Neurosci* 39:197–216.

77. Swanson LW. 2015. *Brain Maps: Structure of the Rat Brain, 4th ed*. (Beta ver. 3.1). www.

larrywswanson.com.

78. Takagishi M, Chiba T. 1991. Efferent projections of the infralimbic (area 25) region of the medial prefrontal cortex in the rat: an anterograde tracer PHA-L study. *Brain Res* 566:26–39.

79. Tamas G, Somogyi P, Buhl EH. 1998. Differentially interconnected networks of GABAergic interneurons in the visual cortex of the cat. *J Neurosci* 18(11):4255–4270.

80. Thompson RH, Swanson LW. 2010. Hypothesis-driven structural connectivity analysis supports network over hierarchical model of brain architecture. *Proc Natl Acad Sci U S A* 107: 15235–15239.

81. Van De Werd HJJM, Uylings HBM. 2008. The rat orbital and agranular insular prefrontal cortical areas: a cytoarchitectonic and chemoarchitectonic study. *Brain Struct Funct* 212:384–401.

82. Van De Werd HJJM, Rajkowska G, Evers P, Uylings HBM. 2010. Cytoarchitectonic and chemoarchitectonic characterization of the prefrontal cortical areas in the mouse. *Brain Struct Funct* 214:339–353.

83. Vertes RP. 2002. Analysis of projections from the medial prefrontal cortex to the thalamus in the rat, with emphasis on nucleus reuniens. *J Comp Neurol* 442:163–187.

84. Vertes RP. 2004. Differential projections of the infralimbic and prelimbic cortex in the rat. *Synapse* 51:32–58.

85. Vogt BA, Peters A. 1981. Form and distribution of neurons in the rat cingulate cortex: areas 32, 24, and 29. *J Comp Neurol* 195:603–625.

86. Yoshida K, McComack S, Espana RA, Crocker A, Scammell TE. 2006. Afferents to the orexin neurons of the rat brain. *J Comp Neurol* 494:845–861.

Vita

Ken Negishi was born in Twin Cities, California. He is the second child of Maria and Ichiro Negishi. He graduated from Burges High School in 2006 and finished his Bachelor of Science degree in Biology in Dec 2013. In Fall 2014 he started his graduate level education at the University of Texas at El Paso, where he worked in Dr. Arshad Khan's laboratory. As a Master's student, he worked as a teaching assistant for Human Anatomy & Physiology I. He is a lover of jazz and cats.

Permanent address: 9455 Viscount Blvd, Apt. # 528
El Paso, TX 79925